Adsorption of mono- and multivalent cat- and anions on DNA molecules.

E. Allahyarov[1], H. Löwen[2] and G. Gompper[1]
1 Institute für Festkörperforschung, Forschungszentrum Jülich, D-52425 Jülich, Germany
2 Institut für Theoretische Physik II, Heinrich-Heine-Universität Düsseldorf, D-40225 Düsseldorf, Germany
(February 2, 2008)

Abstract

Adsorption of monovalent and multivalent cat- and anions on a deoxyribose nucleic acid (DNA) molecule from a salt solution is investigated by computer simulation. The ions are modelled as charged hard spheres, the DNA molecule as a point charge pattern following the double-helical phosphate strands. The geometrical shape of the DNA molecules is modelled on different levels ranging from a simple cylindrical shape to structured models which include the major and minor grooves between the phosphate strands. The densities of the ions adsorbed on the phosphate strands, in the major and in the minor grooves are calculated. First, we find that the adsorption pattern on the DNA surface depends strongly on its geometrical shape: counterions adsorb preferentially along the phosphate strands for a cylindrical model shape, but in the minor groove for a geometrically structured model. Second, we find that an addition of monovalent salt ions results in an increase of the charge density in the minor groove while the total charge density of ions adsorbed in the major groove stays unchanged. The adsorbed ion densities are highly structured along the minor groove while they are almost smeared along the major groove. Furthermore, for a fixed amount of added salt, the major groove cationic charge is independent on the counterion valency. For increasing salt concentration the major groove is neutralized while the total charge adsorbed in the minor groove is constant. DNA overcharging is detected for multivalent salt. Simulations for a larger ion radii, which mimic the effect of the ion hydration, indicate an increased adsorbtion of cations in the major groove.

PACS: 87.15.Aa, 61.20.Ja, 82.70.Dd, 87.10.+e

I. INTRODUCTION

In addition to its biological role as the carrier of genetic information [1], deoxyribose nucleic acid (DNA) in solution exhibits typical polyelectrolyte behavior. Its physico-chemical properties, such as melting temperature, transition between different DNA forms, binding interaction of proteins and other ligands, strongly depend on the added salt concentration in aqueous solution. Some physical properties of DNA, such as its osmotic pressure and activity coefficients [2], can be explained within a simple polyelectrolyte picture of DNA as obtained via counterion condensation theory of Manning [3], Poisson-Boltzmann (PB) theory [4–7] and Monte Carlo simulations [4,8–12] of a homogeneously charged cylinder. Although a cylinder with an effective homogeneous line charge density might be an appropriate model for studying properties far away from the DNA surface, more details are getting relevant if one approaches the DNA surface. These details can be classified in the following way: first the actual *charge distribution* along the DNA molecule is not a homogeneous line charge but a discrete set of phosphate charge groups along a double helix. Next, the *geometric shape* of the DNA including the major and minor grooves between the two phosphate strands is getting relevant. Finally, *molecular details* of the DNA surface should be considered including specific interactions and explicit solvent molecules.

The PB calculations have been successfully applied to investigate the DNA electrostatics, such as the electrostatic field of double-helix charge distribution [13] and of all-atom DNA models [14,15]. The comparison between the simulation and PB results for the multivalent counterion distribution around DNA, addressed in Refs. [4,10,15–17], reveals great differences between them. The reason for such differences is the lack of the hard core and Coulomb correlations in mean-field based PB theory. On the other hand, an all-atom DNA simulations in solution is computationally very costly and can be performed only with small system sizes and low salt concentrations [18–28]. Therefore we focus in this paper on a "primitive approach" [29] which goes beyond the simplistic model of a line-charged cylinder but still does not include full atomic details. The physical reason to do so is that most of the general properties of DNA are expected to result from a combination of Coulomb and excluded volume interactions which are the most dominating parts of the total interactions for long and short ranges [30]. Following this strategy, we disregard the discrete structure of water replacing it by a dielectric background, but treat the salt ions, the double-helical charge pattern on the DNA molecule and the geometrical grooved shape of the DNA molecule explicitly.

This paper focuses on the cat- and anion adsorption pattern on the DNA surface. In particular, in contrast to earlier simulations which only present rotationally averaged data for adsorbed ions [19,31–36], we resolve the adsorption in the major and minor grooves and on the phosphate strands. Both a qualitative and a quantitative knowledge of the adsorption pattern is desirable, since it is needed as a crucial input in other more coarse-grained approaches like the Kornyshev-Leikin (KL) theory of DNA-DNA interaction [37]. It is known that the details of the adsorption pattern strongly influence the effective interaction forces and even governing the sign of the interaction. Hence the adsorption pattern will have direct consequences for aggregation and bundling of DNA molecules caused by an effective mutual attraction [38–40]. It is also known that adding multivalent ions to the solution causes drastic changes in the ion adsorption and in the DNA aggregation and bundling

[41–43]. Many experimental facts have been collected regarding the adsorption of multivalent ions on the DNA. To name just a few, there is experimental evidence indicating that Mn_{2+} and Cd_{2+} condense on DNA [44,45] but Ca_{2+} or Mg_{2+} do not [45,46]. This points to an important specificity [47–51] and the question arising is whether this can be understood in simple terms of effective ion radii. Multivalent counterions of valency larger than 2, on the other hand, such as trivalent spermidine (Spd) and tetravalent spermine (Spm) are believed to play a key role in maintaining cellular DNA in a compact state [52–55]. The compactification of DNA [39,40] seems to be mediated by their adsorption on the DNA surface [39,56,57]. Therefore there is a need to study the role of high-valency counterions in the DNA adsorption pattern in a systematic way.

While the Manning condensation theory on a homogeneously charged cylinder is well-studied by now [58], it is a priori unclear how the adsorbed counterions will partition themselves in the two grooves and on the phosphate strands. Moreover, the adsorption of anions, which carry the same charge as the phosphates, in the major grooves is an interesting issue, in particular for higher counterion valencies.

The goal of this paper is twofold: first, we aim to predict both qualitatively and quantitatively the nature of the adsorption pattern on a single DNA molecule for a given added salt concentration, given microion valencies and microion radii. Ion-specific effects, however, only enter via the ion sphere radius and its charge. Although the actual numbers may be influenced by further details such as the dielectric properties of water at close ion distances, we think that the *trends* of our findings upon a change in ion valency and salt concentration will be robust. In particular for high valency ions, the interactions should be dominated by the Coulombic part such that our "primitive" model should be more appropriate. Second, on a more technical level, we would like to investigate the influence of the geometrical structure of the DNA shape used in the theoretical model of the adsorption pattern. It is expected that a grooved shape will attract more counterions into the grooves electrostatically such that the adsorption pattern will depend on the geometrical shape used in the model.

In our computer simulations we find that the adsorption pattern on the DNA surface depends strongly on the geometrical model shape of the DNA surface. In detail three different shapes, modelling the geometrical structure of the grooves on different levels, are considered. It is found that counterions adsorb preferentially along the phosphate strands for a cylindrical model shape but in the minor groove for a geometrically structured model.

Furthermore, we find that an addition of more monovalent salt ions, provided the counterions are also monovalent, results in an increase of the charge density in the minor groove, while the total charge density of ions adsorbed in the major groove stays unchanged. The adsorbed ion densities are highly structured along the minor groove while they are almost smeared along the major groove.

We also analyze the influence of the ion valency on the ion adsorption pattern on the DNA surface. We show that for any fixed amount of salt the major groove cationic charge is constant for any counterion valency. For added multivalent salt, we show the existence of a major groove neutralization phenomena while the minor groove total charge remains constant.

We also address the DNA overcharging phenomenon, which is of special interest in biology, for example, for the delivery of genes to the living cell for the purpose of the gene therapy. Since both the bare DNA and cell surface are negatively charged, normally DNA

does not approach cell surface. An overscreened DNA molecules, however, is effectively positively charged such that it could pass through the negative cell membrane. Our simulations show that the overcharging of DNA appears generally in multivalent salt solution regardless the counterion valency. Finally we have performed a few simulations with larger ion radii in order to mimic a larger ion hydration shell in the solvent. Our findings show that for an increasing ion radius more cations go to the major groove whereas the minor groove and strand ionic occupations shrink.

The paper is organized as follows: In section II we discuss different models for the DNA shape. Our simulation technique and model parameters are presented in section III. Results are given in section IV. Finally we conclude in section V.

II. DIFFERENT MODELS FOR THE DNA SHAPE

We consider the B-form of DNA which is the most common state of DNA in aqueous solutions. It has an inner core formed by nucleotide pairs, and two sugar-phosphate strands spiraling around the core. The latter forms a well-known double helix with a pitch length of about 34Å and a core radius of about 9Å. There are two phosphate groups per base pair, and 10 base pairs per pitch (or helical turn). The axial rise per base pair along the DNA long axis is 3.4Å , hence there is one elementary charge per each 1.7Å. The average value of the angle between the adjacent base pairs is 36^0 which makes the average distance between neighboring charges on the DNA surface to be 7Å. This distance, which is much smaller than the helical pitch, is of the order of the Debye screening length under physical conditions. Finally the helix persistence length is about 500Å.

Three different models for the DNA shape will be studied here: i) a simple cylinder model (CM), ii) an extended cylinder model (ECM) with a grooved structure and iii) the Montoro-Abascal model (MAM) [33]. The cross sections of these DNA models in the xy plane that is perpendicular to the DNA long axis (z-axis) and hits two phosphates on different strands are sketched in Figure 1 and will be discussed subsequently: in all three models the phosphate charges are discretely placed at certain positions coincident with those of the phosphorus atoms in crystalline DNA.

i) Cylindrical model (CM), see Figure 1a: This model was used by Kornyshev and Leikin [37] and by two of us in another study [59]. In the CM, the cylindrical DNA core possesses a diameter of D=20Å. Two strings of point-like and monovalent phosphate charges of size $d_p = 0.4$Å have cylindrical coordinates $(\rho_i^s, \phi_i^s, z_i^s)$ relevant to the phosphate sites of the B-form of DNA:

$\rho_i^s = D/2$=10Å, $\phi_i^s = \phi_0^s + i \times 36^0$, $z_i^s = z_0^s + i\times$ 3.4Å.

Here s=1,2 specifies the nucleic acid strand, i=0,...,9 describes a full DNA turn and the z-axis is the long DNA axis. Furthermore, $\phi_0^1 = 0^0$, $z_0^1 = 0$ for the first strand ($s = 1$) and $\phi_0^2 = 144^0$, $z_0^2 = 0$ for the second strand ($s = 2$).

ii) Extended cylinder model (ECM), see Figure 1b: As designed by Lyubartsev et. al. [31], both the helical DNA grooves and the discrete charge localization on the DNA surface are incorporated. In the ECM, the DNA molecule has a hard cylindrical core of diameter D=17.8Å, which is slightly smaller than in the CM. The phosphate charges are swollen up to hard sphere of diameter d_p=4.2Å explicitly forming grooves. Other DNA parameters are similar to the CM.

iii) Montoro-Abascal model (MAM), see Figure 1c: This more elaborate model was first introduced in Ref. [33] where the grooved structure of DNA is increased by adding another neutral sphere between the cylindrical core and the charged phosphate sphere. In detail, the inner DNA cylindrical core of D=7.8Å is overwinded by two strings of overlapping spheres. The outer string of monovalently charged phosphate spheres are centered at a radial coordinate of 8.9Å. The radial position of inner string of neutral spheres is 5.9Å. Both spheres have the same ϕ and z coordinates and diameter d_p=4.2Å to incorporate a grooved geometry for the DNA molecule. Clearly, such a design of an overlapped cylinder and two spheres creates a more grooved DNA profile with a deeper cavity in the center of the minor groove. For other details of the MAM and its reliability, we reference the reader to the original papers [33–35].

III. SIMULATION TECHNIQUE AND SYSTEM PARAMETERS

In our simulation set-up, the B-DNA molecule is located in the center of a cubic simulation box. The cylinder axis is parallel to the z-axis and crosses the xy plane at position $\vec{R}$ $(L/2, L/2, 0)$. The size L of the simulation box was chosen to be $L = 102$Å, corresponding to three full turns of B-DNA with a pitch length P=34Å and with $N_p = 3 \times 20 = 60$ phosphate groups along the DNA [34]. There is a small shift in the z-coordinate of two discrete phosphate charges belonging to two different helices of Δz=0.78Å.

Periodic boundary conditions are applied in all three directions, hence the DNA replicas in the z-direction produce an infinitely long DNA molecule, and an infinite array of DNA replicas in neighboring cells is simulated. The phosphate spheres are monovalent, i.e. their charge $q_p < 0$ corresponds to one elementary charge $|e|$, $q_p = -|e|$, and they have an effective diameter d_p which is a variable parameter in our different shape models. In addition to the DNA phosphates, the system contains N_c counterions with charge q_c, and $N_s \equiv N_+ \equiv N_-$ pairs of salt ions of concentration $C_s = N_s/V'$ with charges q_+ and q_-. Here V' is the free volume in the simulation box accessible for these small ions, where the excluded volume of the DNA molecule has been subtracted. The counterion number N_c in the simulation box is fixed by the charge of the DNA molecule due to the constraint of global charge neutrality, $N_c q_c = 60|q_p|$. For simplicity, we shall always deal with a symmetric salt case, $|q_+| = |q_-|$. All small ions are modelled as hard spheres of (hydrated ion) diameter d_c. For most of our simulations, d_c=3Å, but we have obtained data for larger ion sizes d_c=6Å and d_c=8Å as well. The whole system is held at room temperature $T = 298K$. The dielectric constant $\epsilon = 78$ of the solvent is assumed to be uniform throughout the suspension (same value inside the DNA molecule and in the suspending medium), which avoids electrostatic images.

The interactions between the mobile ions and the phosphate charges are described within the framework of the primitive model as a combination of excluded volume and Coulomb interactions reduced by the dielectric constant ϵ of the solvent. The corresponding pair interaction potential between the different charged hard spheres is

$$V_{ij}(r) = \begin{cases} \infty & \text{for } r \leq (d_i + d_j)/2 \\ \frac{q_i q_j e^2}{\epsilon r} & \text{for } r > (d_i + d_j)/2 \end{cases}, \tag{1}$$

where r is the inter-particle separation and i, j are indices denoting the different particle species. Possible values for i and j are c (for counterions), $+, -$ (for positively and nega-

tively charged salt ions), and p (for phosphate groups). In addition, there is an interaction potential V_i^0 between the DNA hard cylinder and the free ions $i = c, +, -$ which is of simple excluded volume form such that these ions cannot penetrate into the cylinder. Similar excluded volume potential exist for the inner neutral DNA spheres in the elaborated MAM. Finally, the ionic strength I and the Debye screening length λ_D of the solution are defined as $I = \frac{1}{2}(q_c^2 N_c/V' + \sum_{j=+,-} q_j^2 C_s)$ and $\lambda_D = \sqrt{\frac{\epsilon k_B T}{4\pi I}}$. In order to compute the statistical averages over the mobile microions, we have performed conventional NVT molecular dynamics simulations, where the long-range electrostatic forces were treated according to the Lekner procedure [59,60]. A typical simulation snapshot of the system is given in Figure 2.

Our major goal is to calculate the mobile ion number densities $\rho_j(\vec{r})$ $(j = c, +, -)$ around the DNA molecule. They are defined as a statistical average,

$$\rho_j(\vec{r}) = \langle \sum_{i=1}^{N_j} \delta(\vec{r} - \vec{r}_i^{\,j}) \rangle. \tag{2}$$

Here $\{\vec{r}_i^{\,j}\}$ denote the positions of the ith particle of species j. The canonical average $< ... >$ over an $\{\vec{r}_i^{\,j}\}$-dependent quantity $\mathcal{A}$ is defined via the classical trace

$$\begin{aligned} \langle \mathcal{A} \rangle = \frac{1}{\mathcal{Z}} \Big\{ \prod_{k=1}^{N_c} \int d^3 r_k^c \Big\} \Big\{ \prod_{m=1}^{N_+} \int d^3 r_m^+ \Big\} \Big\{ \prod_{n=1}^{N_-} \int d^3 r_n^- \Big\} \\ \mathcal{A} \exp\big(-\beta \sum_{i=c,+,-} [V_i^0 + \sum_{j=c,p,+,-} U_{ij}]\big). \end{aligned} \tag{3}$$

Here $\beta = 1/k_B T$ is the inverse thermal energy (k_B denoting Boltzmann's constant) and

$$U_{ij} = (1 - \frac{1}{2}\delta_{ij}) \sum_{l=1}^{N_i} \sum_{k=1}^{N_j} V_{ij}(\mid \vec{r}_l^{\,i} - \vec{r}_k^{\,j} \mid), \tag{4}$$

is the total potential energy of the counter- and salt ions provided the phosphate groups are at positions $\{\vec{r}_n^{\,p}\}$ $(n = 1, ..., N_p)$. Note that the periodically repeated particles are incorporated implicitly in the interaction energy. Finally the prefactor $1/\mathcal{Z}$ in Eq.(3) ensures a correct normalization, $< 1 >= 1$.

In computer simulations and different theoretical approaches the distance below which the ions are considered to be condensed is usually assumed to be in the range of one or two water molecule diameters. Thus the width of the condensation shell near the DNA surface is around 7Å in Manning theory [3], whereas a value of 5Å was invoked in other papers [19,31,61,62]. These values are larger than the thickness of the Stern layer $d_l = A/4\pi\lambda_B$=2Å including ions bound to the molecular surface. Here $\lambda_B = e^2/\epsilon k_B T$ is the Bjerrum length and A is an average area per elementary charge on the molecular surface. In our study we follow the latter criterion and treat the ions as condensed if the *surface-to-surface distance* between the ion sphere and the DNA hard surface is not larger than 2Å. In other words, we are interested in the population in special areas of the DNA surface by small ions rather than the actual ion condensation on the DNA surface [63]. In order to resolve the adsorbed ions along the strands and in the major and minor grooves, we integrate the ion density fields as given by Eqn.(2) over a small volume close to the DNA surface. This volume is bounded by the parallel surface to the DNA surface at distance δ =2Å+$d_c/2$ and has a height ξ in

z-direction. The volume follows the helical symmetry of the DNA molecule. A schematic view of this condensation shell and the definition of the groove and strand adsorption paths around the DNA are given in Figure 3. We have separately counted cations, that comprise of counterions and positively charged salt ions, and anions (coions). The angular-resolved cation and anion density profiles along the phosphate strands and the minor and major grooves represent the main results of this paper. We call a plot of the densities versus polar angle a "panoramic" view of the density profiles and shall present exhaustive data for these quantities for different parameters in the next section. Additionally we define the charge densities of adsorbed ions by $\rho^{(+)} = \sum_{j=c,+} q_j \rho_c^{(j)}$ and $\rho^{(-)} = q_- \rho_c^{(-)}$, where $\rho_c^{(j)}$ are the number densities of the adsorbed ions of species $j \in \{c, +, -\}$.

Our molecular dynamics simulations cover a broad range of salt concentrations from 0.1Mol/l to 1.61 Mol/l, where the latter corresponds to 2000 salt ions of both charges in the simulation box. Details of the simulated states are summarized in Table I. During the simulation we checked that there was a continious exchange of the adsorbed and free ions, which demonstrates that our systems are in equilibrium.

IV. RESULTS

A. Monovalent ions

Let us first discuss monovalent ions. For the extended cylindrical model (ECM), a panoramic angular cat- and anion distribution over $0 < \phi < 2\pi$ is plotted in Figure 4 for the system parameters $q_c = 1$, $q_s = 1$ (Set 1 of Table I) and $C_s = 0.1$Mol/l. The cations cluster in front of the charged phosphates, almost in a site-binding like manner [32–35], showing a strong structuring, while the minor-groove cation density is less structured. The smallest cation density is in the major groove. The anion densities in the DNA grooves and on the phosphate strands are considerably smaller and not structured at all. The major groove population of anions is higher than that in the minor groove and on the strands. The same quantities are shown for the cylinder model (CM) and the Montoro-Abascal model (MAM) in Figures 5 and 6 respectively. As compared to the ECM, an increase of condensed cations along the phosphate strands at the expense of their accumulation in the minor and major grooves is clearly visible for the CM. In the most realistic MAM, however, more cations bind and locate in the DNA grooves [64,65] at the expense of their accumulations on strands. Such an ion relocation from the strands into the grooves entails an entropy gain for salt ions. In the MAM the population of condensed cations along the strands is less by a factor of two as compared to the structured minor groove density. Our conclusion arising from Figures 4, 5, and 6 is twofold: first, on a technical level, the inclusion of a grooved shape in the excluded volume of the DNA molecule is crucial for ion adsorption. It completely changes the charge and structure of the adsorption pattern. Second, taking the MAM as the most realistic description of the DNA shape, we can conclude that adsorbed cations exhibit a pronounced spatial structure along the minor groove. This strong structuring of cations in the minor groove will induce also a structuring of the water molecules in the minor groove and might therefore be related to the so-called "spine of hydration in the minor groove" which is attributed to a high water ordering there [18,66–70]. In general, the spine of hydration emerges due to the occasional intruding of counterions to the particularly electro-negative

regions in the minor groove [71] and is addressed in Refs. [26,34,48,49,69,72–74]. We think that the experimentally measured hydration pattern can be a fingerprint of cation ordering in the minor groove [68,75,76].

The dependence of the adsorption pattern on the salt concentration is shown in Figure 7. The added monovalent salt concentration C_s is increased from 0.2 Mol/l to 1.61 Mol/l for $q_c = 1$, $q_s = 1$ (Set 1). The highest cationic occupation is again in the minor groove but more anions condense in the major groove as the salt density is increased [35]. The total major groove charge, calculated as a difference between the cation (dashed line) and anion (dashed line with symbols) densities in the major groove, is almost independent of the amount of added salt, see the single arrows in Figure 7. In other words, for any monovalent salt density the geometry of major groove and the electrostatic field of the two adjacent phosphate strands regulate the cation and anion populations and keep the major groove charge unchanged. On the other hand, the minor groove is positively charged as the bulk salt density increases, see the difference between the full line and the full line with symbols for different salt densities in Figure 7. The visible cation structuring in the major groove at dense salt, see the right side of Figure 7, is consistent with the experimental evidence for recurring hydration patterns in the major groove [74,77,78]. The other observation is a constancy of the gap between the minor and the major groove cationic occupancies shown in Figure 7 by the double arrows for different salt densities. Obviously in solutions, where the DNA phosphate charges are effectively screened out, it is the osmotic pressure of salt that pushes ions close to the DNA surface. We note that the constancy of the accumulated charge in the major groove and the constancy of the difference between cationic populations of major and minor grooves do not appear in the ECM and CM.

We finally remark that throughout all runs it was revealed that, a distance 5Å -7Å away from the DNA surface a cylindrical symmetry of radial ion distribution is completely restored in accordance with observations of Refs. [31,34,36,79]. Thus the effect of discreteness of DNA charges on counterion concentration profile is generally small and dwindles a few angstroms away from the DNA surface [80,81].

B. Multivalent counterions and monovalent salt

We now consider the case of multivalent counterions and a monovalent salt, for which the Coulomb correlations between the counterions and the DNA phosphates are strong. We keep the salt concentration fixed and increase the counterion valency. This leads to a higher on-strand adsorption of couterions which implies less condensation in the minor and major groove, see Figures 8a. Also for high counterion valencies, the cation adsorption on the minor groove is higher than that on the major groove in accordance with Ref. [82]. The same trends appear also in the ECM and in the CM.

Furthermore, for increasing counterion valency, Figure 8b reveales that the total adsorbed charge in the major groove is *almost constant* while it is getting more positive in the minor groove. The increase of the adsorbed cations in the minor groove causes a visible spatial structuring along the minor groove, see the surging oscillations in Figures 8a and 8b. Again, such an ion structuring is perhaps connected to the experimentally observed spine of hydration. Note that the number of adsorbed ions in the major groove drastically decreases

in the CM and ECM for higher counterion valencies, which reaffirms the crucial role of the modelling of the DNA shape.

C. Multivalent counterions and multivalent salt

For fixed *divalent* salt concentration and increasing counterion valency, similar results are obtained as shown in Figure 9. The number of adsorbed cations decreases in the grooves, see Figure 9a, the total charge in the major groove stays constant (very close to its value in Figure 8b) while it is rising slightly in the minor groove, see Figure 9b. Hence we conclude that total major groove charge is independent of valencies of both cations and anions.

We now increase gradually the amount of added divalent salt. The in-groove ion distributions are shown in Figure 10 for three different salt concentrations. There are two remarkable effects for increasing salt concentration: first the total charge of ions adsorbed in the *major* groove is approaching zero, i.e. *the major groove is neutralized* for high salt concentration. Second, the total charge in the *minor* groove is pretty robust against an increase in salt concentration, see the length of the arrows in Figure 10. The effect of major groove neutralization are lost if a less realistic DNA shape is used as shown in Figure 11 for the CM and the ECM.

In Figure 12, the ion densities adsorbed on the strands are shown for trivalent counterions as a function of divalent salt concentration. The total charge adsorbed along the strands increases with added salt concentration. Togther with the constancy of the minor groove and the neutralization of the major groove this produces an overcharging effect of the DNA which is discussed in the next subsection.

D. Overcharging effect

Charge inversion (also known as an overcharging, overneutralization or charge reversal) is possible for a variety of macroions, ranging from the charged surface, charged lipid membranes to colloids, DNA and actin. It is believed that for this effect to occur, the cations have to be multivalent to enhance the nonlinear effects, such as Coulomb correlations. Thus, in the presence of multivalent ions, the ionic cloud may not only compensate the polyion charge, but even exceed it, resulting in opposite values of the electrostatic potential at some distances. Overcharging has been observed in Monte-Carlo simulation [10,83–85], HNC calculations [86–88] and modified PB theories with nonlinear correlations included [89–91]. In detail, we consider a "physical" overcharging [35,92], when the sign of total charge of the complex of macroion and small ions, which are localized in a thin shell around the macroion, is opposite to the sign of bare macroion charge. Our definition of overcharging differs therefore from the counterion or so-called Z-ion induced "structural" overcharging [93–98] which does not account for the adsorbed salt ions and disappears as more salt is added to solution [99].

During the simulations the charge compensation parameter of DNA phosphate charges, defined as

$$\theta(r) = \left(q_c\rho_c(r) + q_+\rho_+(r) + q_-\rho_-(r)\right)/N_p|q_p|\,, \tag{5}$$

was calculated. Here $N_p = 60$ is the number of phosphate charges in the simulation box. The parameter $\theta(r)$ accounts for the integrated total charge at distance r away from the DNA surface and has the following physical meaning. For $\theta(r) < 1$, the DNA molecule is seen as a negatively charged rod at distance r from its surface. Otherwise, if $\theta(r) > 1$, the effective DNA charge at distance r from its surface is positive. Data for θ are plotted in Figure 13 for the MAM and different salt densities. The denser the salt, the stronger the DNA screening. A qualitatively similar picture to Figure 13 appears for the ECM and CM and different counterion valencies. There is no DNA overcharging in a solution of monovalent salt and multivalent counterions, see the left-hand side of Figure 13 . For divalent salt,which is shown in the right-hand side of Figure 13, and low salt densities the compensation parameter is monotonic, resembling the monovalent salt case. However for dense salt $\theta > 1$ in the DNA vicinity. At the highest salt density involved in our simulations, C_s=1.61 Mol/l, there are even several subsequent overcharging layers: within the layer closest to DNA surface the effective charge is positive, then within the second layer the effective DNA charge is negative, and finally within the third layer the effective charge becomes again positive, see the full line in the right-hand side of Figure 13. We mention that similar overcharging pictures are obtained for the divalent and trivalent counterions in solution with a divalent salt. Thus, summarizing the results of Figure 13 we arrive at the conclusion that it is rather the multivalency of salt ions, than the multivalency of counterions which governs DNA overcharging. Our simulations also show that an overcharging with divalent salt in the CM pops up only for multivalent counterions.

E. Varying the ion radius

The ion size has the meaning of a hydrated ion diameter and is an adjustable parameter of the model that includes effects of the molecular nature of the solvent in an averaged sense. The monovalent counterions are less solvated than divalent cations, the latter condense via their solvent ligands to H-bonds on a DNA surface [100–102]. Since we omit the ion chemisorption and do not account for specific ion effects as exemplified by the Hofmeister effect [103–106], only an electrostatic interaction with the phosphate backbone is taken into account. A small change of the ion size, just in the range of the typical values of the hydrated ion diameters, may cause a transition to an attractive DNA-DNA interaction with a spontaneous assembly of DNA system into an ordered phase [41]. Therefore the hydrodynamic ion size affects the ion correlations and the ion condensation on DNA surface, which are important contributions to the electrostatic potential around the DNA molecule [107,108].

We vary the hydrodynamic radii of solvated ions between 3Å and 8Å [80,109]. The simulation results for three different ion diameters, d_c=3Å, 6Å, 8Å are shown in Figure 14. The gap between the cationic groove occupations decreases as the ion radius increases. Furthermore, more cations go to the major groove whereas the minor groove and the strand ionic occupations shrink. In total, a small amount of cations and anions condense on the DNA surface. Nevertheless all qualitative findings obtained for ions with diameter d_c=3Å and outlined in the previous section, retain valid for twice enlarged ion size d_c=6Å. A further increase of the ionic size up to d_c=8Å, however, makes the ion intrusion into the minor groove a very rare event. The major groove cationic charge then exceeds the minor groove cationic

charge, see the right-hand side of Figure 14. Thus the salt ions "physically" can not explore the full details of the elaborated DNA model. In other words, the salt ions start to "feel" the MAM shape as a less elaborated DNA model, like the ECM. Thus the simulation results for the MAM with d_c=8Å qualitatively resemble the results for the ECM with d_c=6Å or d_c=3Å.

V. CONCLUSIONS

In this work we have studied several models of a DNA polyelectrolyte system containing a mixture of mono- and multivalent ions within the framework of a continuum dielectric approach. We have neglected the granular nature of water and concentrated only on electrostatics of the ion condensation on the DNA surface. Summarizing the results obtained, we have first shown that the small ion condensation pattern on the DNA surface strongly depends on the geometry of the DNA model used. While in the simple cylindrical model cations predominantly bind to the phosphate strands, in the more realistic Montoro-Abascal model the minor groove becomes the principal site of cationic binding. Our simulation results also indicate that the anion condensation is less sensitive to the DNA model shape. We have further investigated the occupancy and charging of DNA grooves as function of increasing cation valency.

We find that the adsorbed ion pattern change with increasing counterion valency is as follows:
i) the cations leave both the major and minor grooves to the phosphate strands,
ii) there are more cations in the minor groove than in the major groove exhibiting a structuring reminiscent to the spine of solvation,
iii) the accumulated cationic charges in the major groove are almost independent of the counterion valency.

An increase in salt concentration leads to the following effects:
for monovalent salt,
i) the *major* groove keeps its total charge at a constant value,
ii) there is a constant cationic charge asymmetry between the DNA grooves,
for multivalent salt,
iii) the *minor* groove keeps its total charge at a constant value,
iv) the major groove is getting neutralized and a DNA overcharging occurs.

All these trends represent important information for the implementation of more phenomenological theories for the interaction between two DNA molecules such as the Kornyshev-Leikin theory [37] where the number of condensed ions on the phosphate strands and on the grooves is a key input quantity. As our results indicate, however, one cannot assume constant fractions of adsorbed ions when the salt concentration and/or the counterion valency is varied.

Let us finally discuss some improvements of our model which could be done step by step in a more realistic description of DNA. First we assume that the persistence length of DNA does not depend from the added salt concentration in order to fit our set up of infinitely stiff single DNA [110–121]. The effect of added salt on the DNA stifness can be taken into account only in simulations with finite DNA fragments. Second, refinement of the present models may account for the specific short-range ion-DNA interactions, or

specific "bonding" of ions to the DNA surface, on the basis of an effective ion-ion and ion-DNA interactions [36,122]. Such chemisorption is believed to contribute to the force-angle dependence, which could be lasted over distances larger the Debye length, 15Å-30Å [37,123,124]. Third, and maybe most important of all, the solvent granularity and the space-dependent dielectric constant were disregarded completely [23,41,72,79,80,125–133]. Fortunately, in most applications, the dielectric discontinuity and dielectric saturation effects have canceling influences in such properties as the energy or the number of condensed ions. That is why the use of a homogeneous solvent with a constant ϵ is believed to be not as crude as it seems from the first point of view [134,135]. Therefore we believe that the general trends found in our study will be stable with respect to a more realistic description of the solvent.

The other experimentally inspired issue is the mechanics of B-DNA which allows the minor groove to open and close to accommodate a divalent cations [100]. The work to account for this effect as well as the ion chemisorption in the major groove is an objective of future work.

ACKNOWLEDGMENTS

E. A. thanks R. Podgornik for fruitful discussions of some results of this paper. We thank the DFG for financial support.

REFERENCES

[1] W. Saenger, *Principles of Nucleic Acid Structure*, Springer-Verlag, New-York, 1984.
[2] A. Katchalsky, Pure Appl. Chem. **26**, 327 (1971).
[3] G. S. Manning, Q. Rev. Biophys. **11**, 179 (1978); G. S. Manning, Acc. Chem. Res. **12**, 443 (1979).
[4] P. Mills, C. F. Anderson, M. T. Record, J. Phys. Chem. **89**, 3984 (1985).
[5] P. L. Hansen, R. Podgornik, V. A. Parsegian, Phys. Rev. E. **64**, 021907 (2002).
[6] R. A. Marcus, J. Chem. Phys. **23**, 1057 (1955).
[7] R. Fuoss, A. Katchalsky, S. Lifson, Proc. Natl. Acad. Sci. USA **37**, 579 (1951); T. Alfrey, P. Berg, H. Morawitz, J. Polym. Sci. **7**, 543 (1951).
[8] C. S. Murthy, R. J. Bacquet, P. J. Rossky, J. Phys. Chem. **89**, 701 (1985).
[9] P. Mills, M. D. Paulsen, C. F. Anderson, M. T. Record Jr., Chem. Phys. Lett. **129**, 155 (1986).
[10] V. Vlachy, A. D. J. Haymet, J. Chem. Phys. **84**, 5874 (1986).
[11] M. D. Paulsen, B. Richey, C. F. Anderson, M. T. Record Jr., Chem. Phys. Lett. **139**, 448 (1987).
[12] M. D. Paulsen, C. F. Anderson, M. T. Record, Biopolymers **27**, 1249 (1988).
[13] P. J. Lin-Chung, A. K. Rajagopal, Phys. Rev. E **52**, 901 (1995).
[14] F. Fogolari, P. Zuccato, G. Esposito, P. Viglino, Biophys. J. **76**, 1 (1999).
[15] J. L. Hecht, B. Honig, Y. K. Shin, W. L. Hubbell, J. Phys. Chem. **99**, 7782 (1995).
[16] S. S. Zakharova, S. U. Egelhaaf, L. B. Bhuiyan, D. Bratko, J. R. C. van der Maarel, J. Chem. Phys. **111**, 10706 (1999).
[17] T. Das, D. Bratko, L. B. Bhuiyan, C. W. Outhwaite, J. Chem. Phys. **99**, 410 (1995).
[18] M. Feig, B. M. Pettitt, Biopolymers **48**, 199 (1998).
[19] M. Feig, B. M. Pettitt, Biophys. J. **77**, 1769 (1999).
[20] M. C. Olmsted, C. F. Anderson, M. T. Record Jr, Proc. Natl. Acad. USA **86**, 7766 (1989).
[21] M. C. Olmsted, J. P. Bond, C. F. Anderson, M. T. Record, Biophys. J. **68**, 634 (1995).
[22] S. A. Allison, J. Chem. Phys. **98**, 12091 (1994).
[23] L. Yang, A. Weerasinghe, B. M. Pettitt, Biophys. J. **69**, 1519 (1995).
[24] G. Lamm, G. R. Pack, J. Phys. Chem. B **101**, 959 (1997); G. Lamm, G. R. Pack, Biopolymers **34**, 227 (1994).
[25] B. Jayaram, D. L. Beveridge, Annu. Rev. Biophys. Biomol. Struct. **25**, 367 (1996).
[26] B. Jayapura, K. A. Sharp, Biopolymers **28**, 975 (1989).
[27] M. A. Young, D. L. Beveridge, J. Mol. Biol. **281**, 675 (1998).
[28] J. N. M. Gurlie, S. C. Harrison, Nature **373**, 257 (1995).
[29] J.-P. Hansen, H. Löwen, Annual Reviews of Physical Chemistry, **51**, 209 (2000).
[30] A. M. J. J. Bonvin, Euro. Biophys. J. **29**, 57 (2000).
[31] A. P. Lyubartsev, L. Nordenskiöld, J. Phys. Chem. B **101**, 4335 (1997).
[32] N. Korolev, A. P. Lyubartsev, A. Rupprecht, L. Nordenskiöld, Biophys. J. **77**, 2736 (1999).
[33] J. C. G. Montoro, J. L. F. Abascal, J. Chem. Phys. **103**, 8273 (1995).
[34] J. C. G. Montoro, J. L. F. Abascal, J. Chem. Phys. **109**, 6200 (1998).
[35] J. L. F. Abascal, J. C. G. Montoro, J. Chem. Phys. **114**, 4277 (2001).
[36] L. E. Guldbrand, T. R. Forester, R. M. Lynden-Bell, Mol. Phys. **67**, 473 (1989).

[37] A. A. Kornyshev, S. Leikin, Proc. Natl. Acad. Sci. USA **95**, 13579 (1998); Phys. Rev. Lett. **82**, 4138 (1999).
[38] R. Netz, Eur. Phys. J. E **5**, 557 (2001).
[39] H. Deng, V. A. Bloomfield, J. M. Benevides, G. J. Thomas Jr, Nucleic Acids Research **28**, 3379 (2000).
[40] M. Deserno, A. Arnold, C. Holm, Macromolecules **36**, 249 (2003).
[41] A. P. Lyubartsev, L. Nordenskiöld, J. Phys. Chem. **99**, 10373 (1995).
[42] H. Deng, V. A. Bloomfield, J. M. Benevides, G. J. Thomas Jr, Nucleic Acids Research **28**, 3379 (2000).
[43] H. Deng, V. A. Bloomfield, Biophys. J. **77**, 1556 (1999).
[44] D. A. Knoll, M. D. Fried, V. A. Bloomfield, *DNA and its Drug Complexes*, edited by R. H. Sarma and M. H. Sarma, Adenin Press, New-York, p.123 (1988).
[45] D. C. Rau, V. A. Parsegian, Biophys. J. **61**, 260 (1992); *ibid* **61**, 246 (1992).
[46] V. A. Bloomfield, Curr. Opin. Struct. Biol. **6**, 334 (1996).
[47] N. Korolev, A. P. Lyubartsev, L. Nordenskiöld, A. Laaksonen, J. Mol. Biol. **38**, 907 (2001).
[48] N. Korolev, A. P. Lyubartsev, A. Rupprecht, L. Nordenskiöld, Biopolymers **58**, 268 (2001).
[49] N. Korolev, A. P. Lyubartsev, A. Laaksonen, L. Nordenskiöld, Biophys. J. **82**, 2860 (2002).
[50] J. Sponer, J. Leszczynski, P. Hobza, Biopolymers (Nucleic Acid Sciences) **61**, 3 (2002).
[51] J. Duguid, V. A. Bloomfield, J. Benevides, G. J. Thomas Jr, Biophys. J. **65**, 1916 (1993).
[52] S. S. Cohen, *A Guide to Polyamines*, Oxford, Oxford University Press, (1998).
[53] C. W. Tabor, H. Tabor, Annu. Rev. Biochem. **53**, 749 (1984).
[54] H. R. Drew, R. E. Dickerson, J. Mol. Biol. **151**, 535 (1981).
[55] B. G. Feuerstein, N. Pattabiraman, L. J. Marton, Proc. Natl. Acad. USA **83**, 5948 (1986); Nucleic Acids **18**, 1271 (1990).
[56] L. C. Gosule, J. A. Schellman, Nature **259**, 333 (1976); J. Mol. Biol. **121**, 311 (1978).
[57] R. W. Wilson, V. A. Bloomfield, Biochemistry **18**, 2192 (1979); R. W. Wilson, D. C. Rau, V. A. Bloomfield, Biophys. J. **30**, 317 (1980).
[58] M. Le Bret, B. Zimm, Biopolymers **23**, 271 (1984); *ibid* Biopolymers **23**, 287 (1984).
[59] E. Allahyarov, H. Löwen, Phys. Rev. E **62**, 5542 (2000).
[60] J. Lekner, Physica A **176**, 485 (1991); J. Lekner, Mol. Simul. **20**, 357 (1998).
[61] B. Andreasson, L. Nordenskiöld, W. H. Braunlin, J. Schultz, P. Stibs, Biochemistry **32**, 961 (1993).
[62] W. H. Braunlin, T. Drakenberg, L. Nordenskiöld, Biopolymers **26**, 1047 (1987).
[63] M. Deserno, C. Holm, S. May, Macromolecules **33**, 199 (2000).
[64] S. B. Howerton, C. C. Sines, D. van der Veer, L. D. Williams, Biochemistry **40**, 10023 (2001).
[65] L. McFail-lsom, C. C. Sines, L. D. Williams, Current opinion in Struct.Biol. **9**, 298 (1999).
[66] B. Halle, V. P. Denisov, Biopolymers **48**, 210 (1998).
[67] V. P. Denisov, B. Halle, Proc. Natl. Acad. USA **97**, 629 (2000).
[68] M. Soler-Lopez, L. Malinina, J. Liu, T. Huynh-Dinh, J. A. Subirana, J. Biological

Chem. **274**, 23683 (1999).
[69] K. J. McConnell, D. L. Beveridge, J. Mol. Biol. **304**, 803 (2000).
[70] B. Schneider, K. Patel, H. M. Berman, Biophys. J. **75**, 2422 (1998).
[71] M. A. Yang, B. Jayaram, D. L. Beveridge, J. Amer. Chem. Soc. **119**, 59 (1997).
[72] G. R. Pack, G. A. Garrett, L. Wong, G. Lamm, Biophys. J. **65**, 1363 (1993).
[73] E. Rajasekaran, B. Jayaram, Biopolymers **34**, 443 (1994).
[74] M. A. Young, B. Jayaram, D. L. Beveridge, J. Am. Chem. Soc. **119**, 59 (1997).
[75] X. Shui, L. McFail-lsom, G. G. Hu, L. D. Williams, Biochemistry **37**, 8341 (1998).
[76] X. Shui, G. Sines, L. McFail-lsom, D. Van-Derveer, L. D. Williams, Biochemistry **37**, 16877 (1998).
[77] D. B. Tippin, M. Sundaralingam, Biochemistry **36**, 536 (1997).
[78] M. Eisenstein, X. Shakked, J. Mol. Biol. **248**, 662 (1995).
[79] B. Jayaram, K. Sharp, B. Honig, Biopolymers **28**, 975 (1989).
[80] J. Conrad, M. Troll, B. H. Zimm, Biopolymers **27**, 1711 (1988).
[81] D. Hochberg, T. W. Kephart, G. Edwards, Phys. Rev. E **49**, 851 (1994); D. Hochberg, G. Edwards, T. W. Kephart, Phys. Rev. E **55**, 3765 (1997); G. Edwards, D. Hochberg, T. W. Kephart, Phys. Rev. E **50**, R698 (1994).
[82] D. Stigter, Biopolymers **46**, 503 (1998).
[83] G. M. Torrie, J. P. Valleau, J. Chem. Phys. **73**, 5807 (1980).
[84] L. Degreve, M. Lozada-Cassou, E. Sancez, E. Gonzalez-Tovar, J. Chem. Phys. **98**, 8905 (1993); L. Degreve, M. Lozada-Cassou, Mol. Phys. **86**, 759 (1995).
[85] M. Jonsson, P. Linse, J. Chem. Phys. **115**, 3406 (2001).
[86] E. G. Tovar, H. Losada-Cassou, D. Henderson, J. Chem. Phys. **83**, 361 (1985).
[87] H. Greberg, R. Kjellander, J. Chem. Phys. **108**, 2940 (1998); J. Ulander, H. Greberg, R. Kjellander, J. Chem. Phys. **115**, 7144 (2001).
[88] R. Kjellander, S. Marcelja, R. M. Pashley, J. P. Quirk, J. Chem. Phys. **92**, 4399 (1990); H. Greberg, R. Kjellander, J. Chem. Phys. **108**, 2940 (1998).
[89] S. Y. Park, R. F. Bruinsma, W. M. Gelbart, Euro. Phys. Lett. **46**, 454 (1999).
[90] J. F. Joanny, Eur. Phys. J. B **9**, 117 (1999); R. R. Netz, J. F. Joanny, Macromolecules **32**, 9026 (1999); *ibid* Macromolecules **32**, 9013 (1999).
[91] F. A. M. Leermakers, J. M. P. van der Oever, E. B. Zhulina, J. Chem. Phys. **118**, 969 (2003).
[92] M. Deserno, F. Jimenez-Angeles, C. Hohn, M. Lozada-Cassou, J. Phys. Chem. B **105**, (2001); M. Quesada-Perez, E. Gonzalez-Tovar, A. Martin-Molina, M. Lozada-Cassou, R. Hidalgo-Alvarez, Chem. Phys. Chem. **4**, 235 (2003).
[93] R. Messina, C. Holm, K. Kremer, Phys. Rev. Lett. **85**, 872 (2000); Eur. Phys. Lett. **51**, 461 (2000).
[94] M. Patra, M. Patriarca, M. Karttunen, physics/0211006
[95] T. T. Nguyen, A. Yu. Grosberg, B. I. Shklovskii, J. Chem. Phys. **113**, 1110 (2000); B. I. Shklovskii, Phys. Rev, E **60**, 5802 (1999); T. T. Nguyen, A. Yu. Grosberg, B. I. Shklovskii, Phys. Rev. Lett. **85**, 1568 (2000); B. I. Shklovskii, Phys. Rev. Lett. **82**, 3268 (1999).
[96] T. T. Nguyen, B. I. Shklovskii, J. Chem. Phys, **115**, 7298 (2001); A. Yu. Grosberg, T. T. Nguyen, B. I. Shklovskii, Rev. Mod. Phys. **74**, 329 (2002).
[97] R. M. Talingting, Y. Ma, C. Simmons, S. E. Webber, Langmuir **16**, 862 (2000).

[98] P. S. Kuhn, Y. Levin, M. C. Barbosa, Physica A **266**, 413 (1999); *ibid* Physica A **274**, 8 (1999).
[99] E. Allahyarov, H. Löwen, Phys. Rev. E **63**, 041403 (2001).
[100] T. K. Chiu, R. E. Dickerson, J. Mol. Biol. **301**, 915 (2000).
[101] H. A. Tajmir-Riahi, M. Naoui, R. Ahmad, J. Biomol. Struct. Dyn. **11**, 83 (1993); I. Fita, J. L. Campos, L. C. Puigjaner, J. A. Subriana, J. Mol. Biol. **167**, 157 (1983).
[102] P. J. Heath, J. M. Schurr, Macromolecules **25**, 4149 (1992).
[103] B. W. Ninham, V. Yaminsky, Langmuir **13**, 3097 (1997).
[104] A. Tardieu, F. Bonnete, S. Finet, D.Vivares, Acta. Cryst. D **58**, 1549 (2002).
[105] R. Piazza, M. Pierno, J. Phys. Cond. Matter **12**, A443 (2000).
[106] P. Benas, L. Legrand, M. Ries-Kautt, Acta Cryst D **58**, 1582 (2002).
[107] S. Gavryushov, P. Zielenkiewicz, Biophys. J. **75**, 2732 (1998).
[108] D. Stigter, K. A. Dill, Biophys. J. **71**, 2067 (1996).
[109] B. E. Conway, Ionic Hydration in Chemistry and Biophysics, Elsevier p.73 (1981).
[110] L. D. Williams, L. J. Maher III, Annu. Rev. Biophys. Biomol. Struct. **29**, 497 (2000).
[111] Y. Lu, B. Weers, N. C. Stellwagen, Biopolymers **61**, 261 (2002).
[112] G. Ariel, D. Andelman, Phys. Rev. E **67**, 011805 (2003); Europhys. Lett. **61**, 67 (2003).
[113] J. G. Duguid, V. A. Bloomfield, Biophys. J. **69**, 2642 (1995); J. G. Duguid, V. A. Bloomfield et al, Biophys. J. **69**, 2623 (1995).
[114] P. E. Sottas, E. Larquet, A. Stasiak, J. Dubochet, Biophys. J. **77**, 1858 (1999).
[115] M. O. Khan, B. Jönsson, Biopolymers **49**, 121 (1999).
[116] C. G. Baumann, S. B. Smith, V. A. Bloomfield, C. Bustamante, Proc. Natl. Acad. Sci. USA **94**, 6185 (1997).
[117] K. K. Kunze, R. R. Netz, Phys. Rev. E **66**, 011918 (2002).
[118] H. Liu, J. Gapinski, L. Skibinska, A. Patkowski, R. Pecora, J. Chem. Phys. **113**, 6001 (2000).
[119] J. Widom, R. L. Baldwin, J. Mol. Biol. **144**, 431 (1980).
[120] V. A. Bloomfield, Biopolymers **44**, 269 (1997).
[121] R. Golestanian, M. Kardar, T. B. Liverpool Phys. Rev. Letters **82**, 4456 (1999).
[122] B. M. Pettitt, P. J. Rossky J. Chem. Phys. **84**, 5836 (1986).
[123] H. M. Harreis, A. A. Kornyshev, C. N. Likos, H. Löwen, G. Sutmann, Phys. Rev. Lett. **89**, 018303 (2002); Virt. J. Biol. Phys. Research **3**, 12 (2002).
[124] A. G. Cherstvy, A. A. Kornyshev, S. Leikin, J. Phys. Chem. B **106**, 13362 (2002).
[125] P. G. Kusalik, G. N. Patey, J. Chem. Phys. **88**, 7715 (1988).
[126] M. K. Gilson, A. Rashin, R. Fine, B. Honig, J. Mol. Biol. **183**, 503 (1985).
[127] B. Jayaram, S. Swaminathan, D. L. Beveridge, K. Sharp, B. Honig, Macromolecules **23**, 3156 (1990); B. Jayaram, A. Das, N. Aneja, J. Mol. Structure **361**, 249 (1996).
[128] M. A. Young, B. Jayaram, D. L. Beveridge, J. Phys. Chem. B **102**, 7666 (1998).
[129] J. Mazur, R. L. Jernigan, Biopolymers **31**, 1615 (1991).
[130] D. Petsev, B. R. Thomas, S. T. Yau, P. G. Vekilov, Biophys. J. **78**, 2060 (2000).
[131] A. V. Lukashin, D. B. Beglov, M. D. Frank-Kamenetskii, J. Biomolecular Structure and Dynamics **9**, 517 (1991).
[132] J. R. C. van der Maarel, Biophys. J. **76**, 2673 (1999).
[133] The dielectric discontinuity effect for spherical geometry and image charges was recently analysed in R. Messina, J. Chem. Physics **117**, 1 (2002). See also P. Linse, J.

Phys. Chem. **90**, 6821 (1986); G. M. Torrie, J. P. Valleau, G. N. Patey, J. Chem. Phys. **76**, 4615 (1982).
[134] see L. R. Pratt, G. Hummer, A. E. Garsia, Biophys. Chem. **51**, 147 (1994); E. Guardia, R. Rey, J. A. Padro, J. Chem. Phys. **95**, 2823 (1991).
[135] A. P. Lyubartsev, A. Laaksonen, Phys. Rav. E **52**, 3730 (1995).

TABLES

TABLE I. Parameters used for the different simulation sets.

Set	q_c	q_s
Set 1	1	1
Set 2	1	2
Set 3	3	2
Set 4	2	1
Set 5	3	1
Set 6	2	2

FIGURES

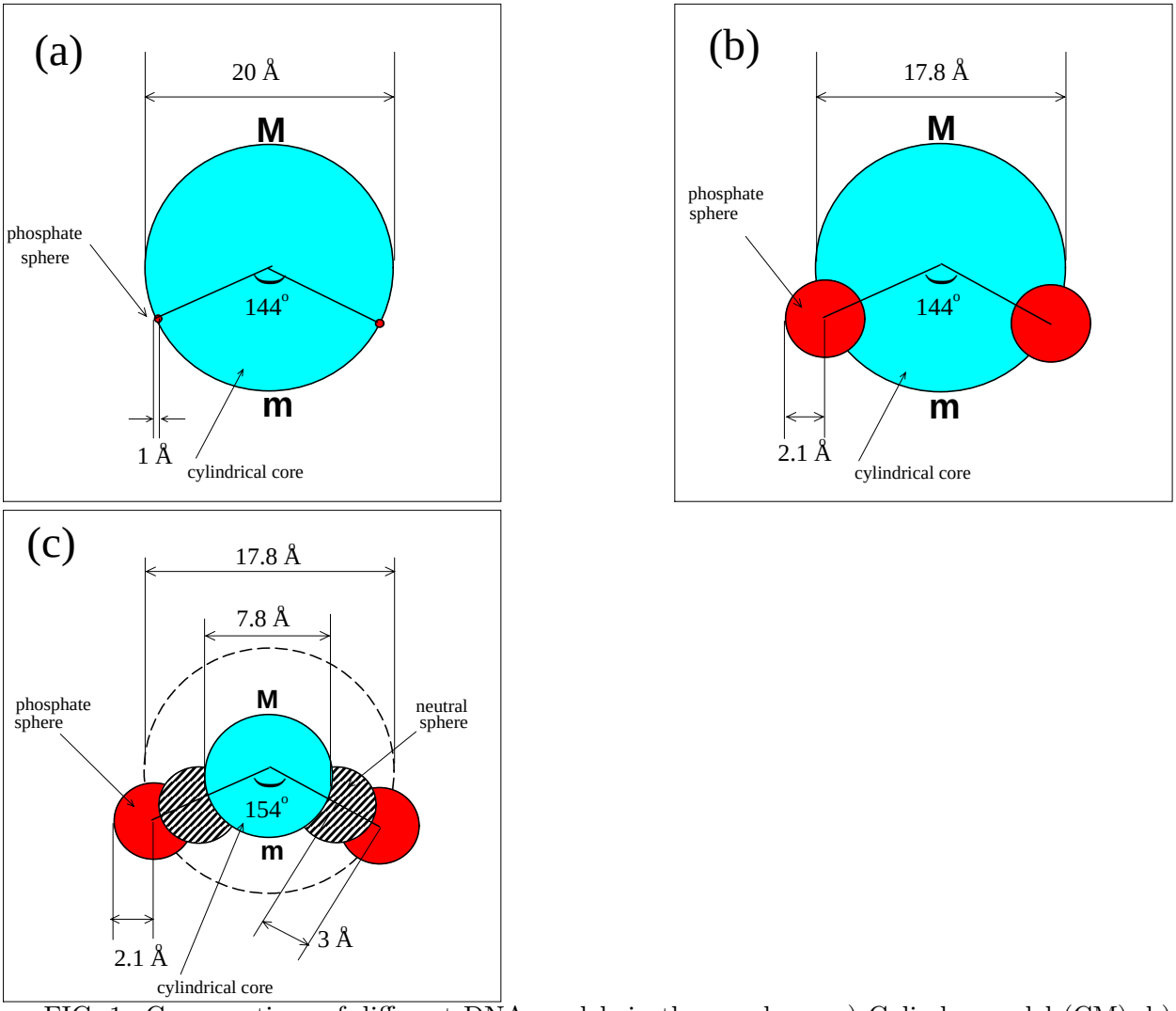

FIG. 1. Cross sections of different DNA models in the xy plane. a) Cylinder model (CM), b) Extended cylinder model (ECM), c) Grooved, or Montoro-Abascal like model (MAM). Phosphate charges are shown as dark spheres. The DNA cylindrical core is colored in gray, the hatched areas correspond to neutral hard spheres. The inscribed letters "M" and "m" denote the major and minor grooves correspondingly.

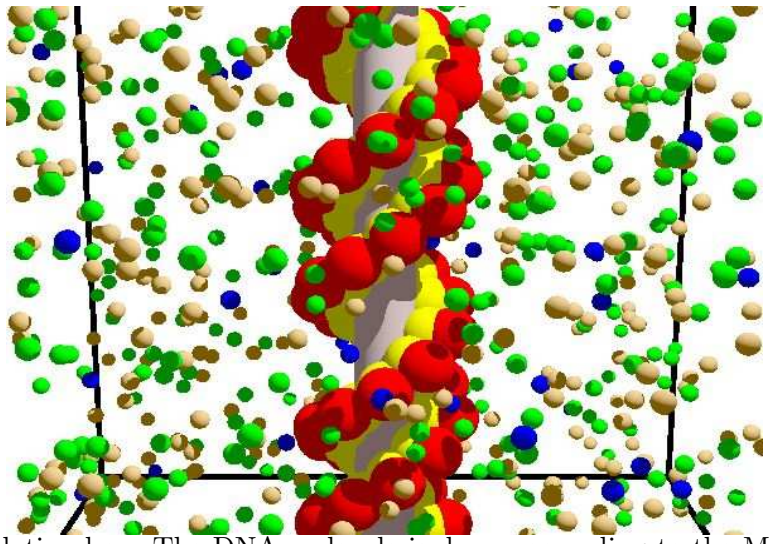

FIG. 2. Snapshot of the simulation box. The DNA molecule is drawn according to the MAM. Black spheres on the DNA strands represent the phosphate charges. Internal grey spheres between the phosphates and the DNA cylindrical core are neutral. Positive (negative) salt ions spreaded across the simulation volume are shown as open (hatched) spheres.

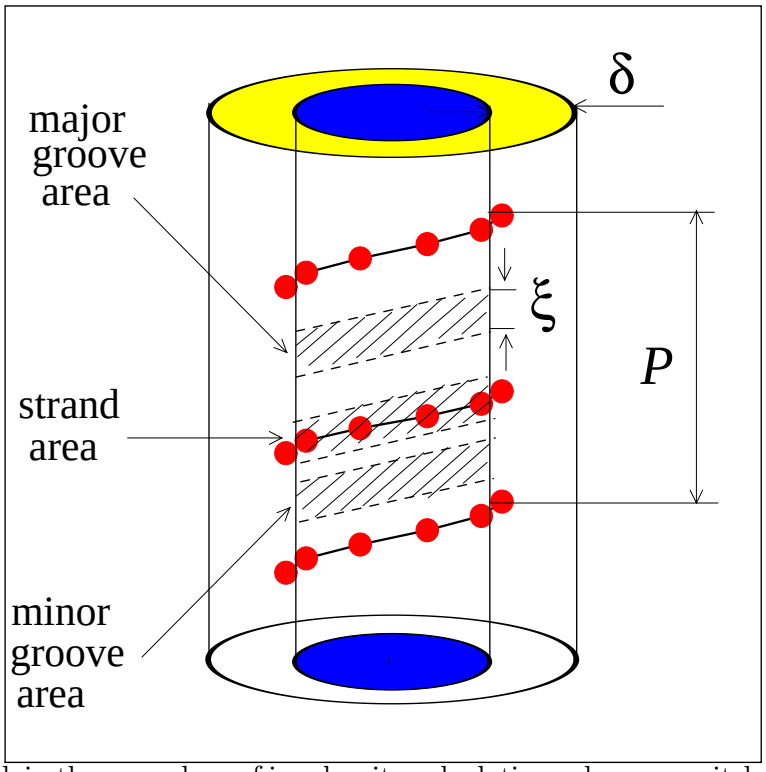

FIG. 3. A schematic picture to explain the procedure of ion density calculations along one pitch length (P) of a DNA molecule. The filled circles connected with full line are phosphate groups. The shaded areas correspond to a path along the major groove, minor groove and one of the phosphate strands. The path height is $\xi = 3.4\mathring{A}$ and width is δ=5Å.

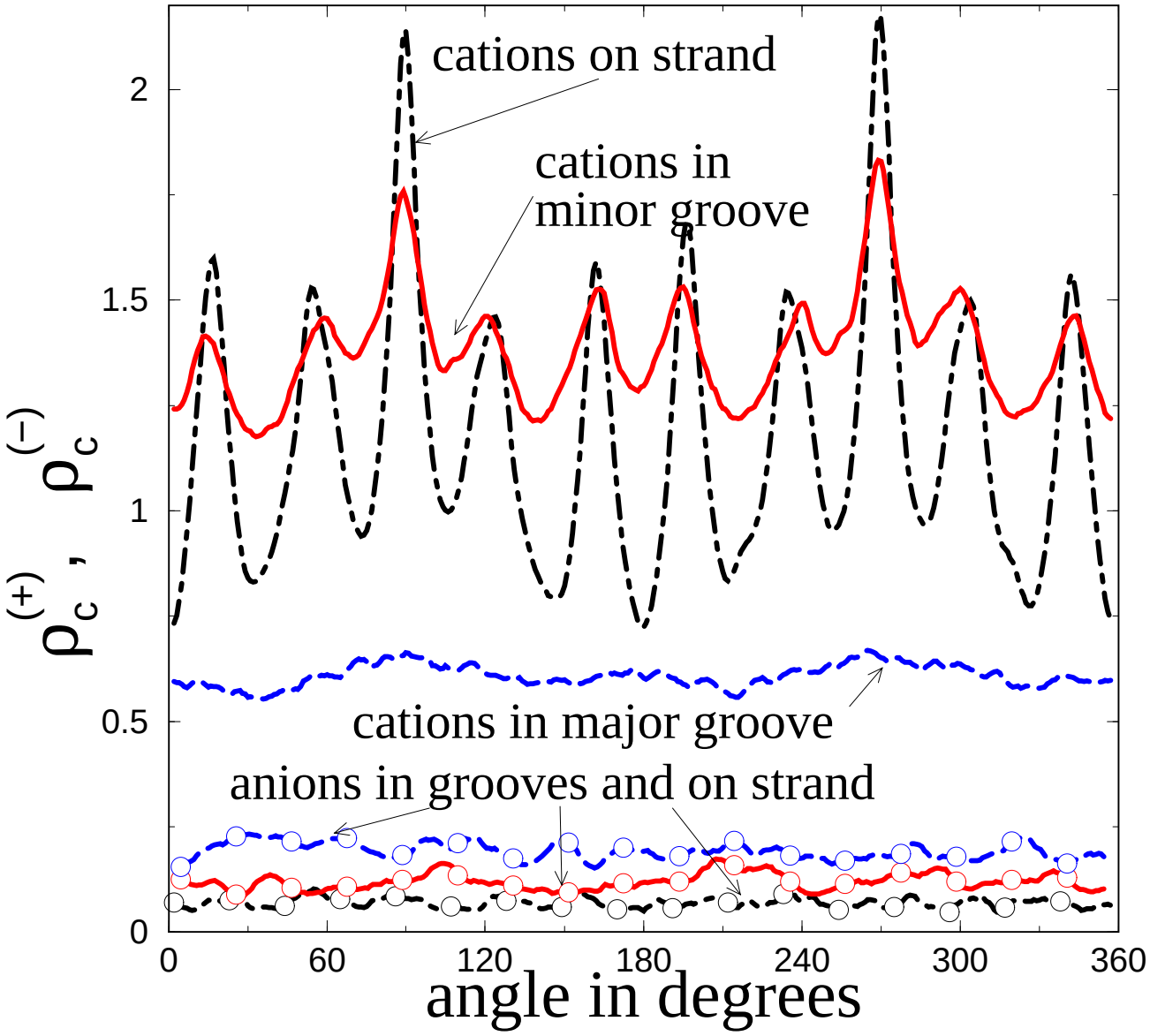

FIG. 4. Panoramic view of the condensed small ion densities near the DNA surface for $q_c = 1$, $q_s = 1$ (Set 1), $C_s = 0.1$Mol/l and the ECM. The density unit is 0.02 Mol/l. Dot-dashed lines: distribution on the phosphate strands, full lines: distribution in the minor groove, dashed lines: distribution in the major groove. Lines without or with symbols correspond to cation $\rho_c^{(+)}$ or anion $\rho_c^{(-)}$ densities. The value of the cation distribution is much larger than the anion distribution (where the latter is enhanced by a factor of 10).

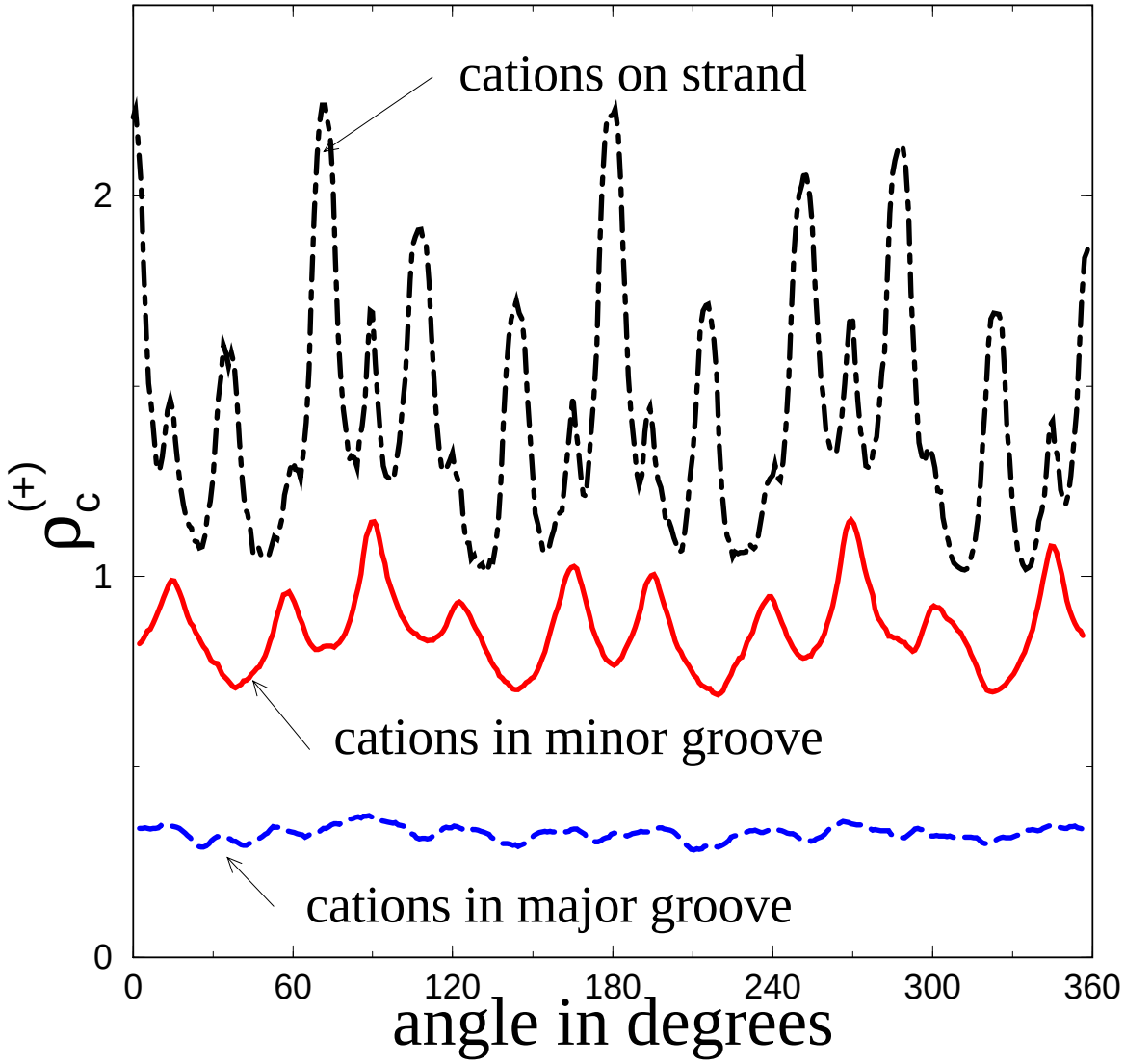

FIG. 5. Panoramic view of the condensed small ion densities near the DNA surface for the cylinder model (CM). The parameters are the same as in Figure 4.

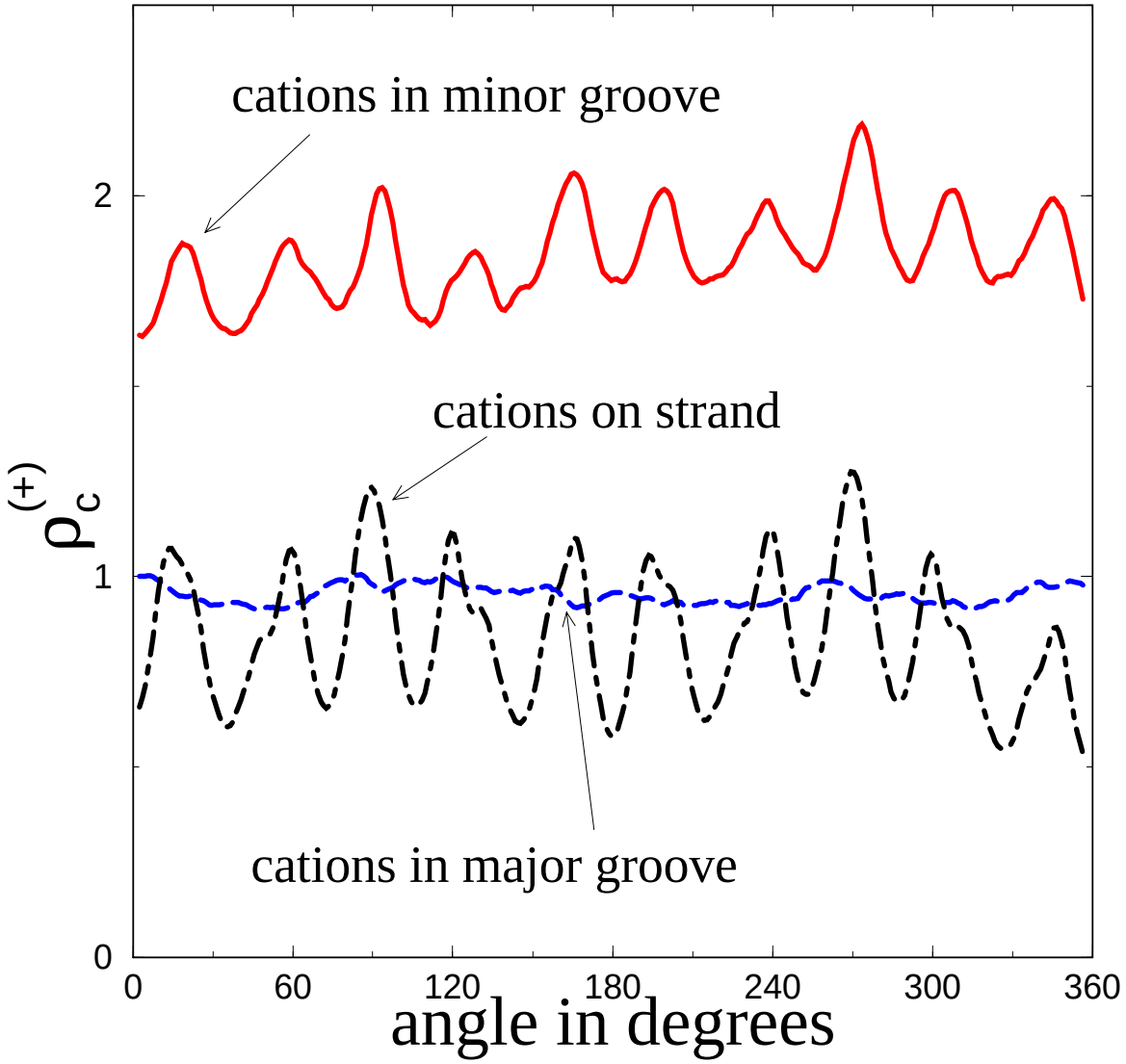

FIG. 6. Panoramic view of the condensed small ion densities near the DNA surface for the Montoro-Abascal model (MAM). The parameters are the same as in Figure 4.

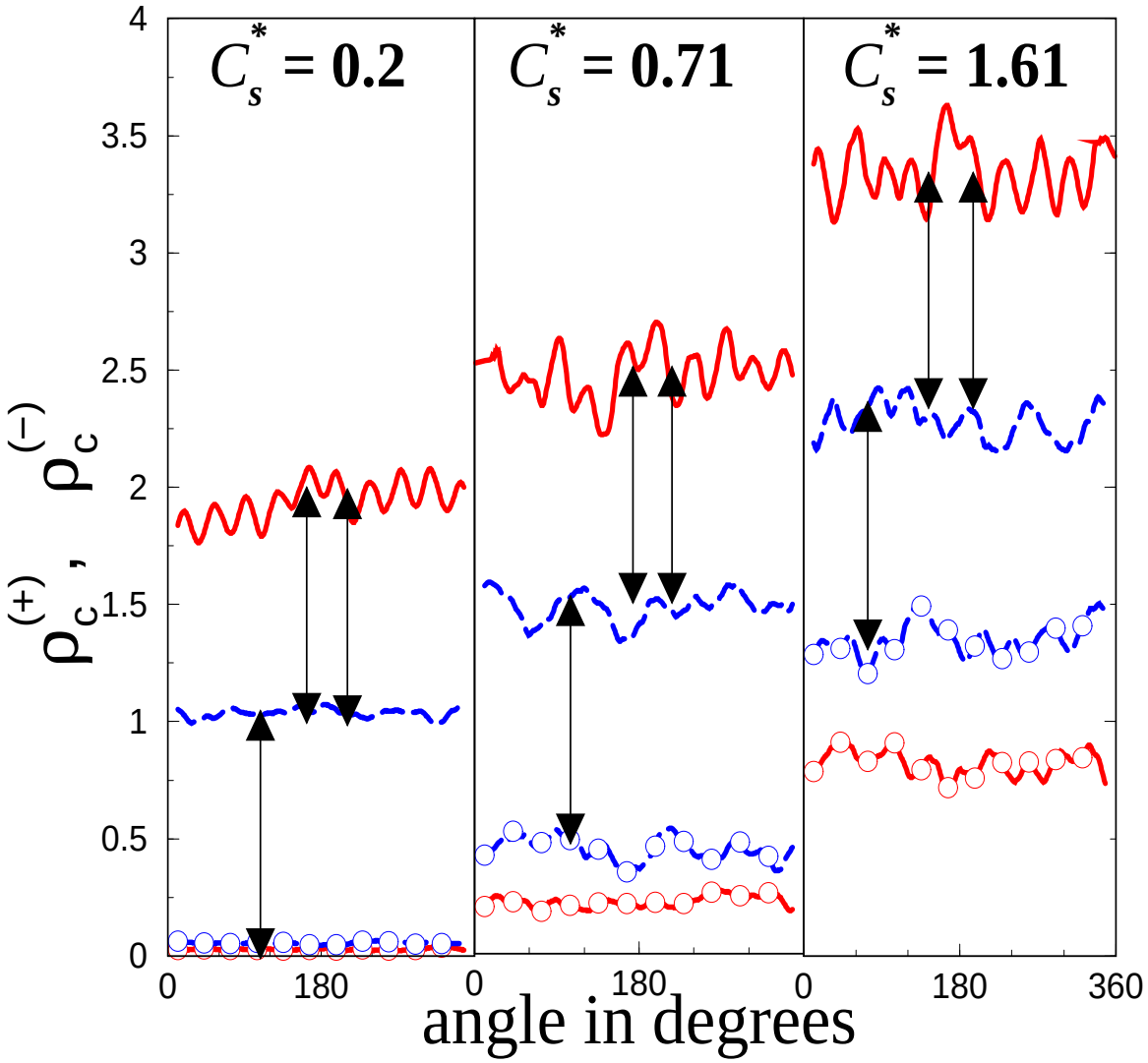

FIG. 7. Panoramic view of ion densities in DNA grooves for MAM and $q_c = 1$, $q_s = 1$ (Set 1). Three full panoramic views along the x axis correspond to three different salt densities; from left to right, $C_s^* = C_s/C_s^0$ =0.2, 0.71, 1.61 with $C_s^0 = 1$Mol/l. Full line- charge distribution in the minor groove, dashed line- charge distribution in the major groove. Lines without or with symbols correspond to cation $\rho_c^{(+)}$ or anion $\rho_c^{(-)}$ densities. The single arrow indicates the constancy of the major groove charge at different added salt densities. The constancy of the difference between the cationic charges of DNA grooves is shown as a double arrow.

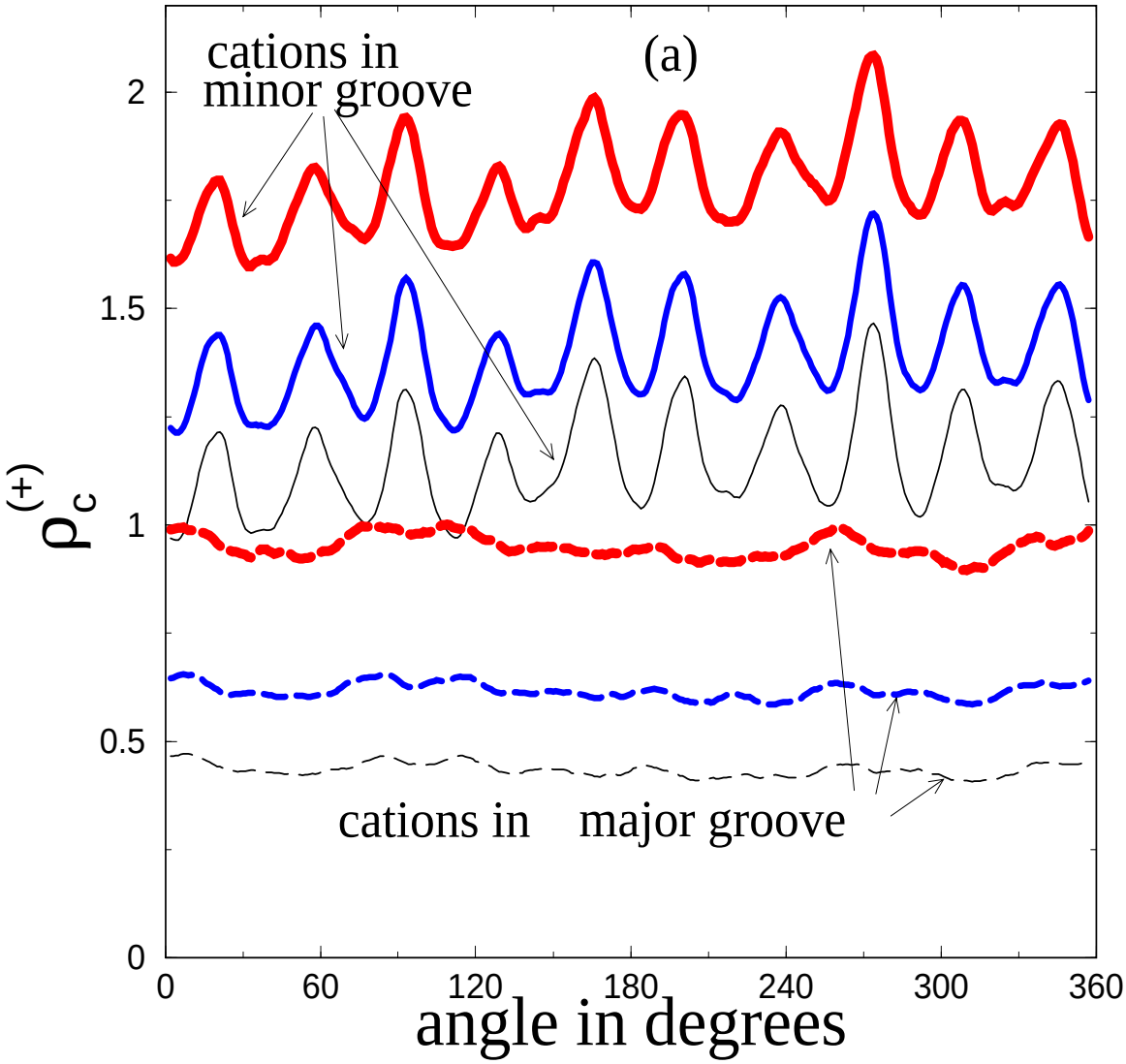
cations in
minor groove
(a)
2
1.5
1
0.5
0
$\rho_c^{(+)}$
cations in major groove
0
60
120
180
240
300
360
angle in degrees

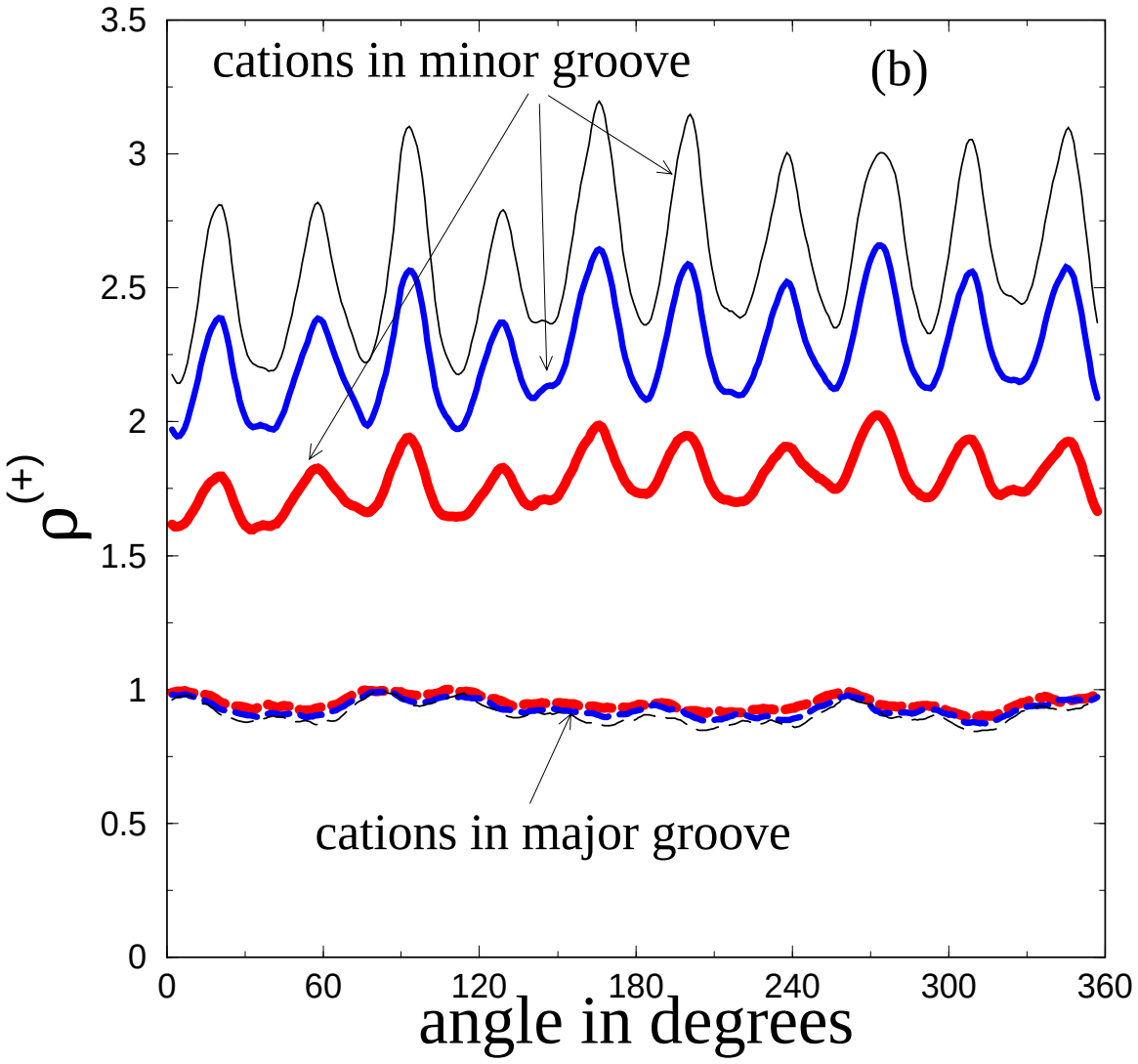

FIG. 8. Panoramic view of the cation number density $\rho_c^{(+)}$ (a) and charge density $\rho^{(+)}$ (b) for the MAM. Monovalent salt C_s =0.1 Mol/l and different counterion valencies. Full line- cations in the minor groove, dashed line- cations in the major groove. Thick lines- monovalent counterions (Set 1), medium sized line- divalent counterions (Set 4), thin line- trivalent counterions (Set 5).

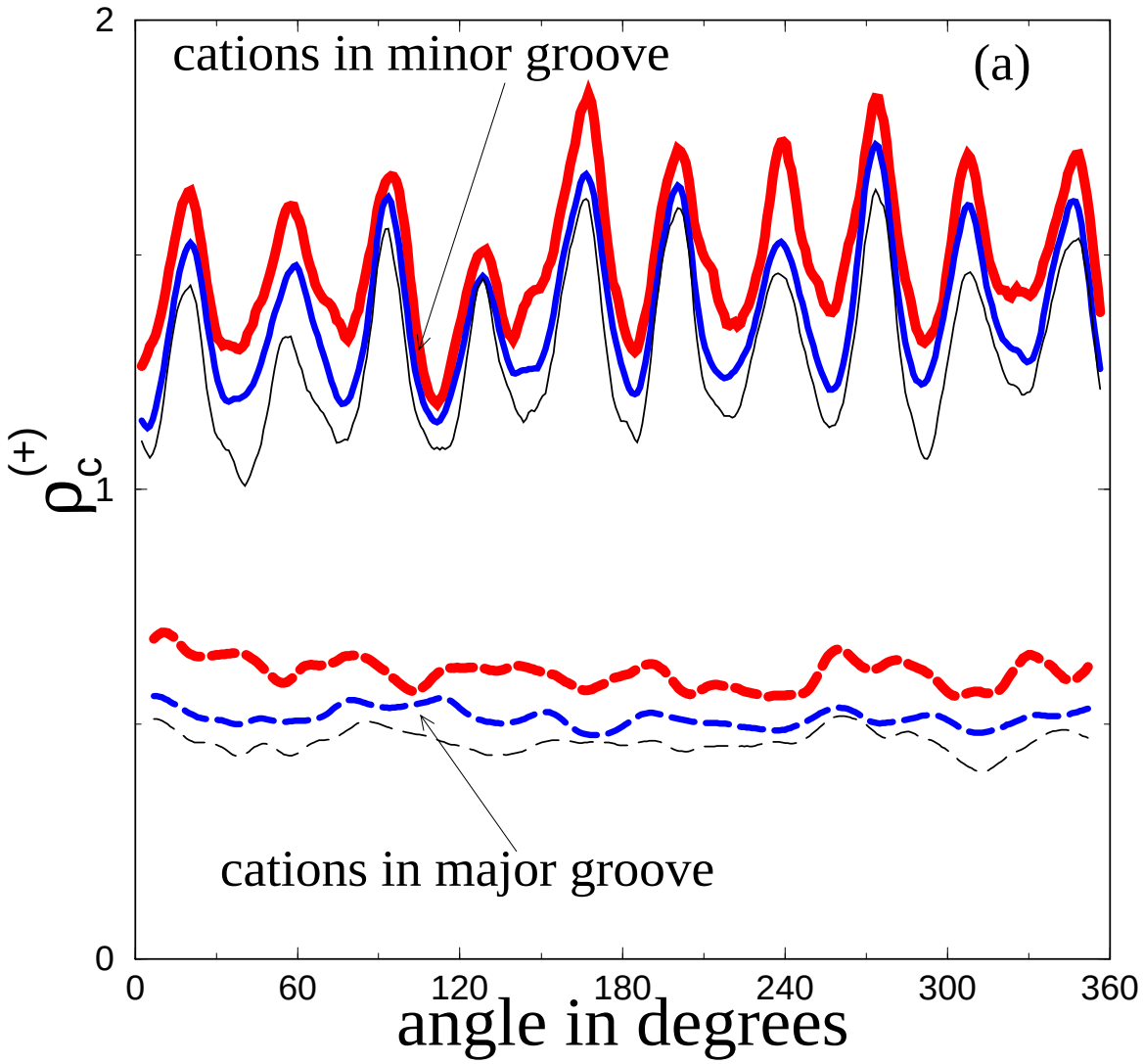
cations in minor groove
(a)
cations in major groove
$\rho_c^{(+)}$
2
1
0
0
60
120
180
240
300
360
angle in degrees

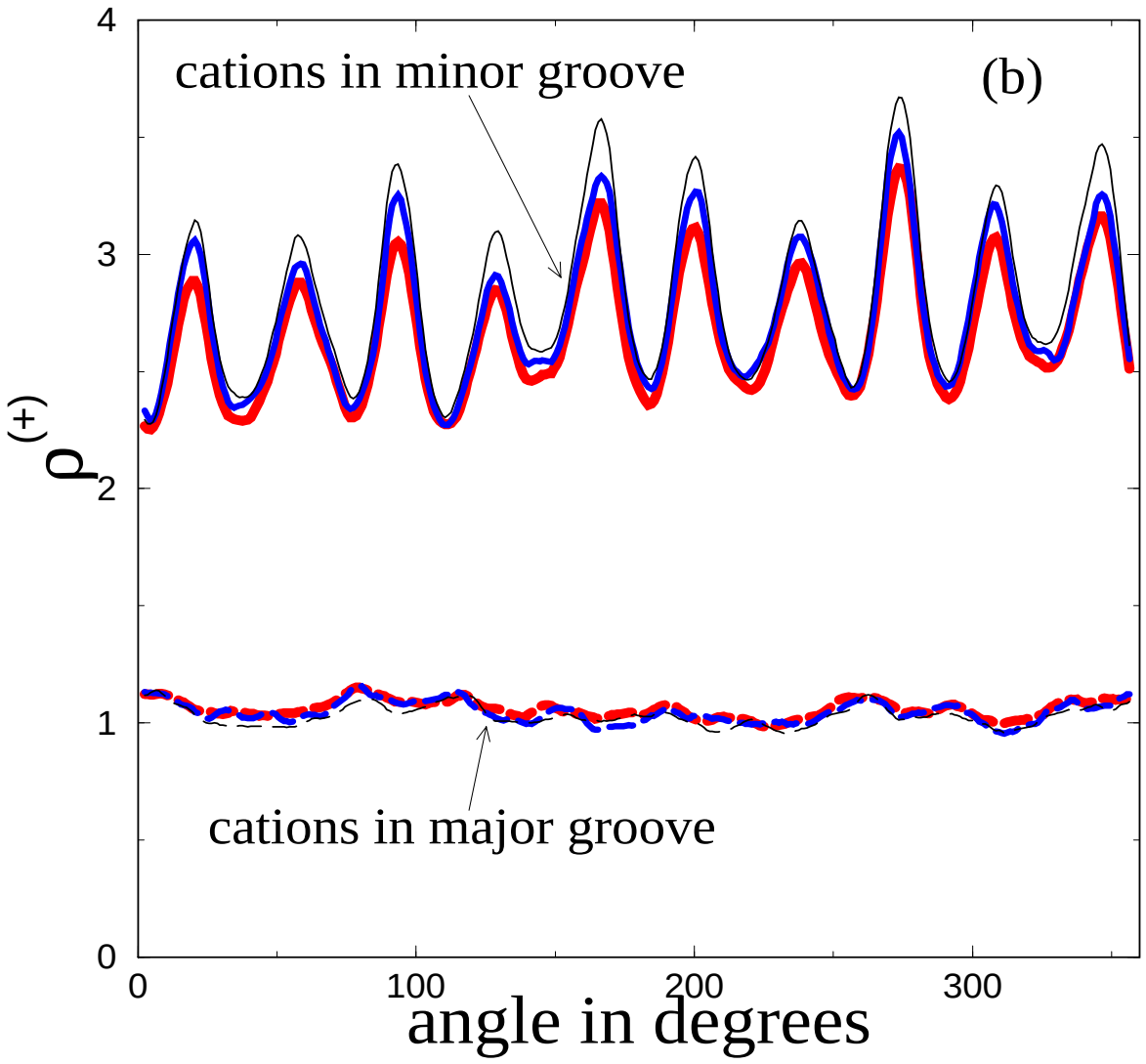

FIG. 9. Panoramic view of the cation number density $\rho_c^{(+)}$ (a) and charge density $\rho^{(+)}$ (b) for the MAM. Divalent salt C_s =0.2 Mol/l and different counterion valencies. Full lines- cations in the minor groove, dashed lines- cations in the major groove. Thick lines- monovalent counterions (Set 2), medium sized line- divalent counterions (Set 6), thin line- trivalent counterions (Set 3).

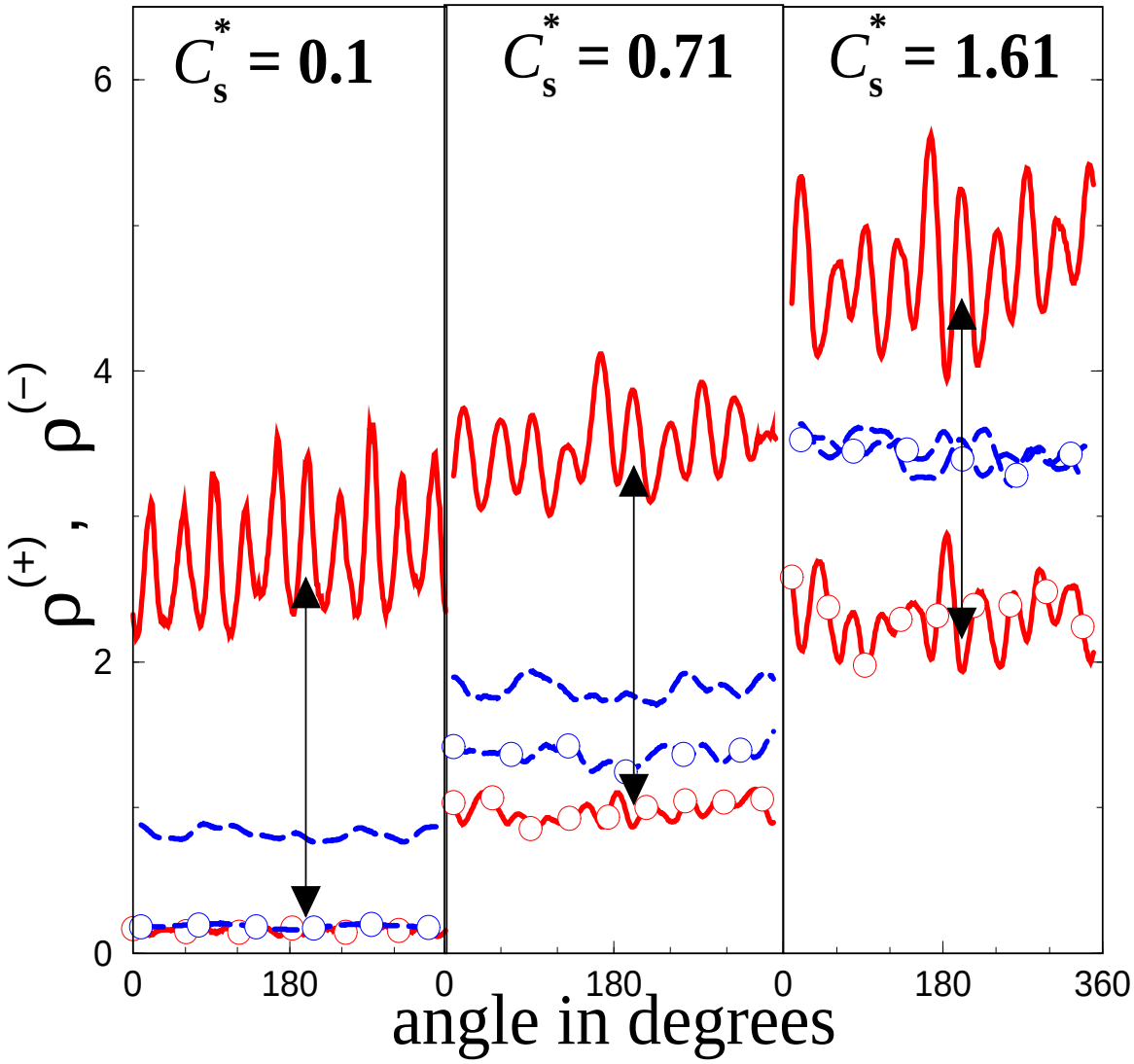

FIG. 10. Panoramic view of ion charge densities in the DNA grooves for the MAM, trivalent counterions and divalent salt (Set 3) and three different salt concentrations; from left to right, $C_s^* = C_s/C_s^0$ =0.1, 0.71, 1.61 with C_s^0 = 1Mol/l. Full line- charge distribution in the minor groove, dashed line- charge distribution in the major groove. Lines without or with symbols correspond to cation $\rho^{(+)}$ or anion $\rho^{(-)}$ charge densities. The shrinking of the gap between the major groove cationic (dashed line) and anionic (dashed line with symbols) charges, as more salt is added, is the onset of the major groove neutralization. The minor groove charge does not depend on the salt concentration, see arrows which indicate the total charge density in minor groove (the gap between the minor groove cation (full line) and anion (full lines with symbols) charges).

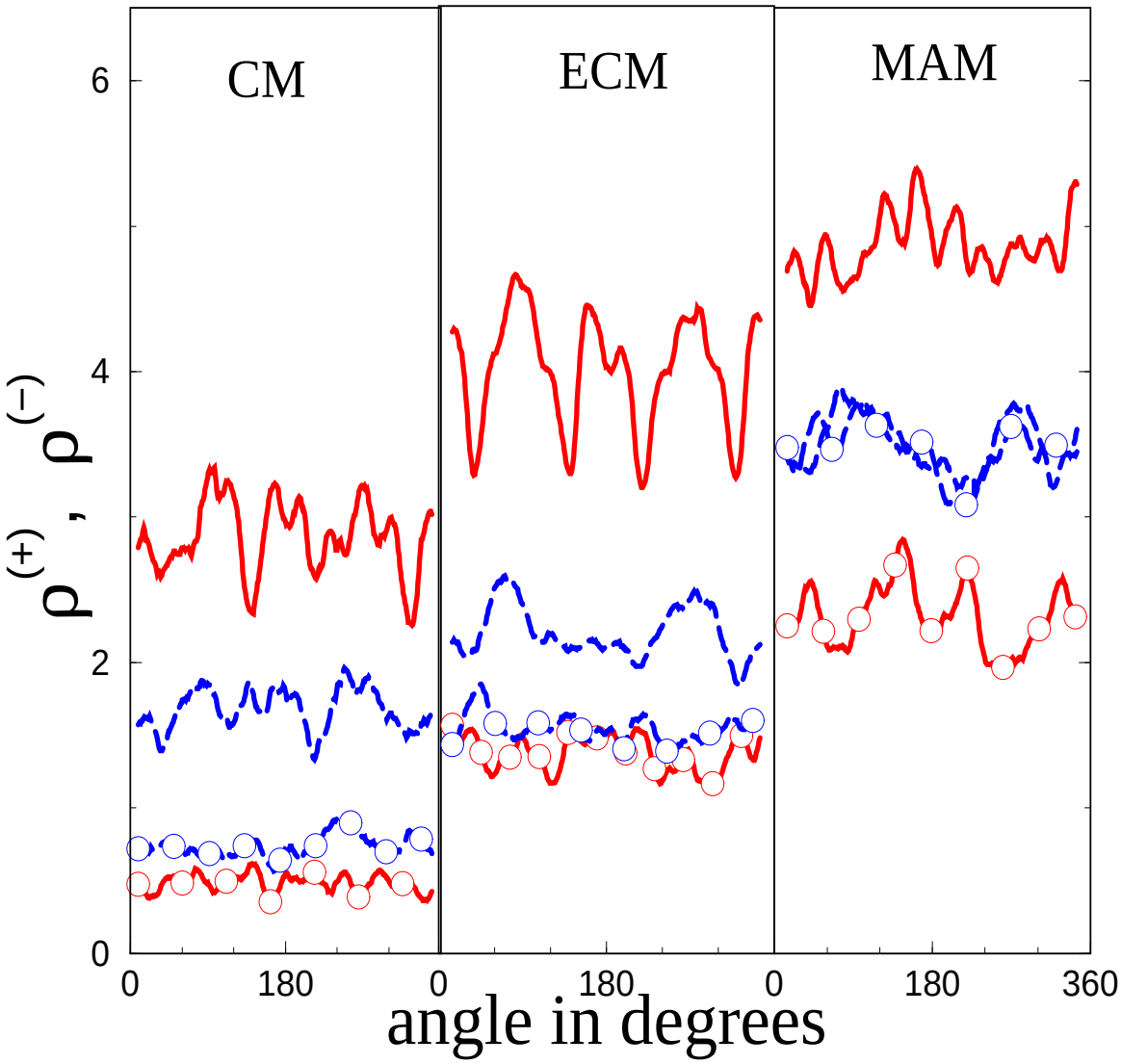

FIG. 11. Panoramic view of ion charge densities in the DNA grooves, monovalent counterions and divalent salt (Set 2) and C_s =1.61 Mol/l. Different DNA models, from left to right: CM, ECM, MAM. Full line- charge distribution in the minor groove, dashed line- charge distribution in the major groove. Lines without or with symbols correspond to cationic $\rho^{(+)}$ or anionic $\rho^{(-)}$ charge densities. Note that the major groove neutralization, described by a coincidence of the major groove cationic (dashed line) and major groove anionic (dashed line with symbols) densities, appears only in the MAM.

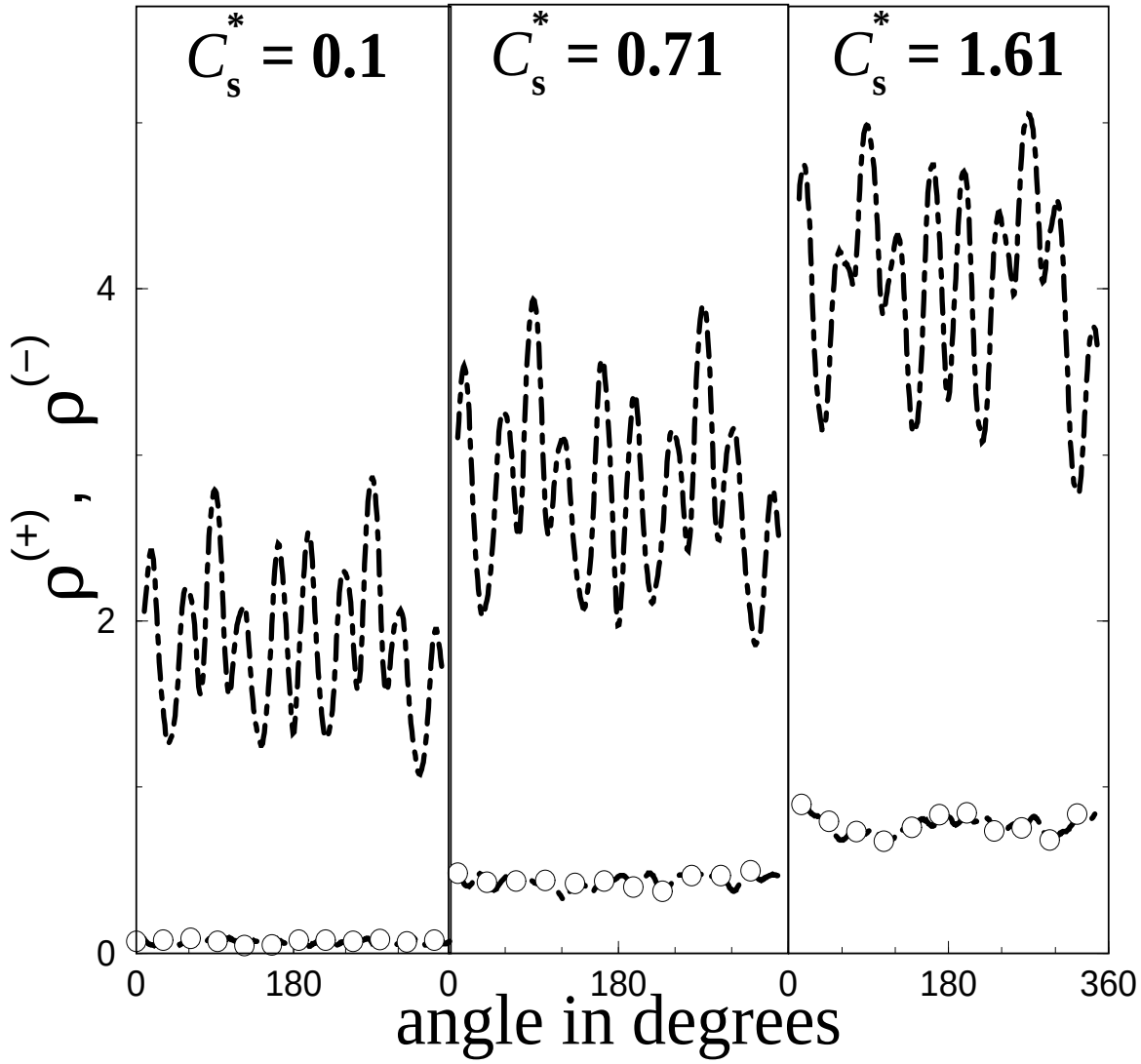

FIG. 12. Panoramic view of ion charge densities on the phosphate strands for the MAM, trivalent counterions and divalent salt (Set 3) and three different salt concentrations; from left to right, $C_s^* = C_s/C_s^0$ =0.1, 0.71, 1.61 with C_s^0 = 1Mol/l. The total ionic charge on strand, defined as a difference between the cationic charge $\rho^{(+)}$ (dot-dashed line) and anionic charge $\rho^{(-)}$ (dot-dashed line with symbols) increases as more salt is added to solution.

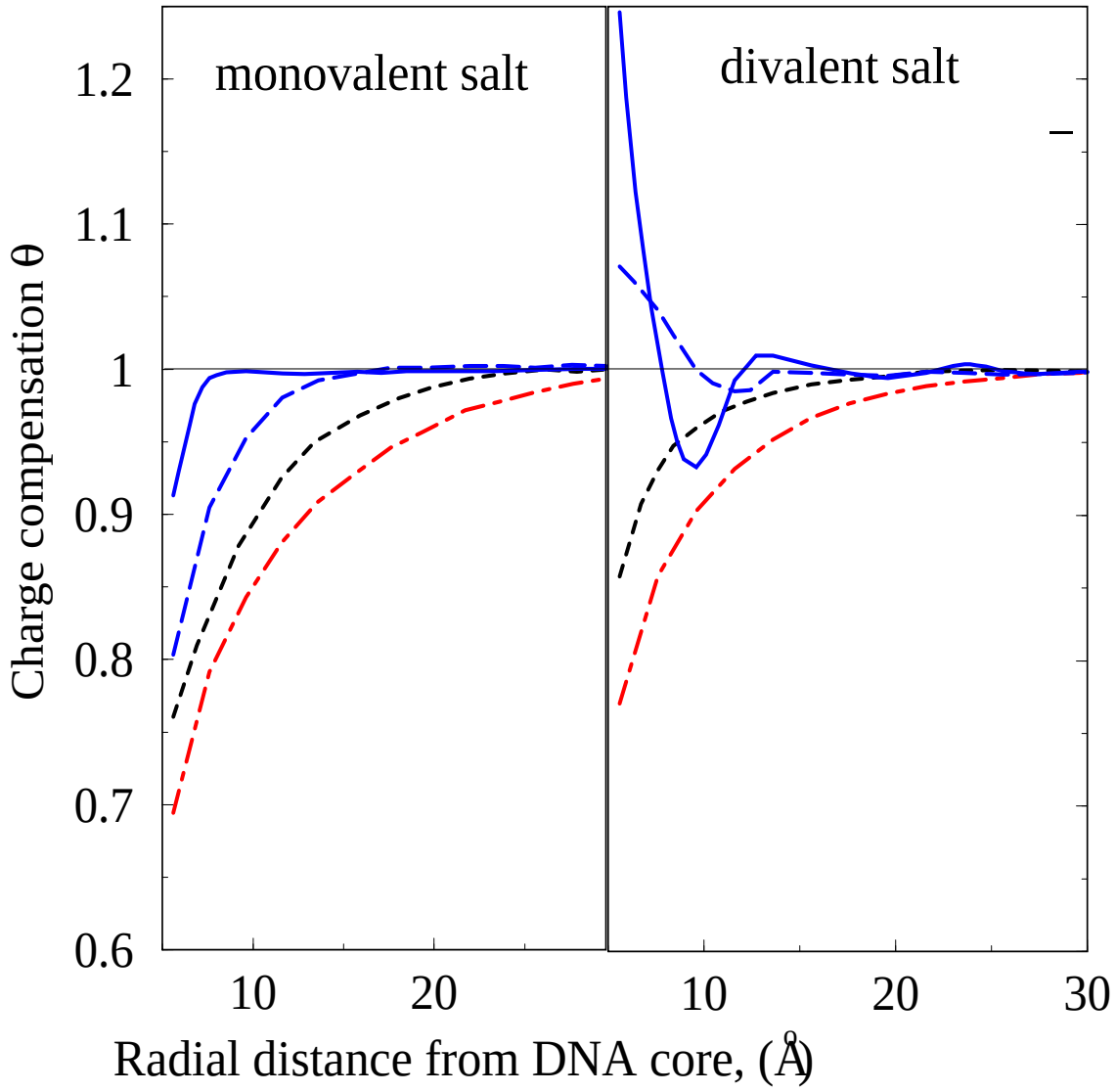

FIG. 13. Charge compensation parameter θ versus distance from the DNA core surface for the MAM and different salt densities. The salt concentration C_s is increased from bottom to top; 0.1 M/l (dot-dashed line), 0.2 M/l (dashed line), 0.71 M/l (long dashed line) and 1.61 M/l (full line). (a) trivalent counterions and monovalent salt (Set 5). (b) monovalent counterions and divalent salt (Set 2).

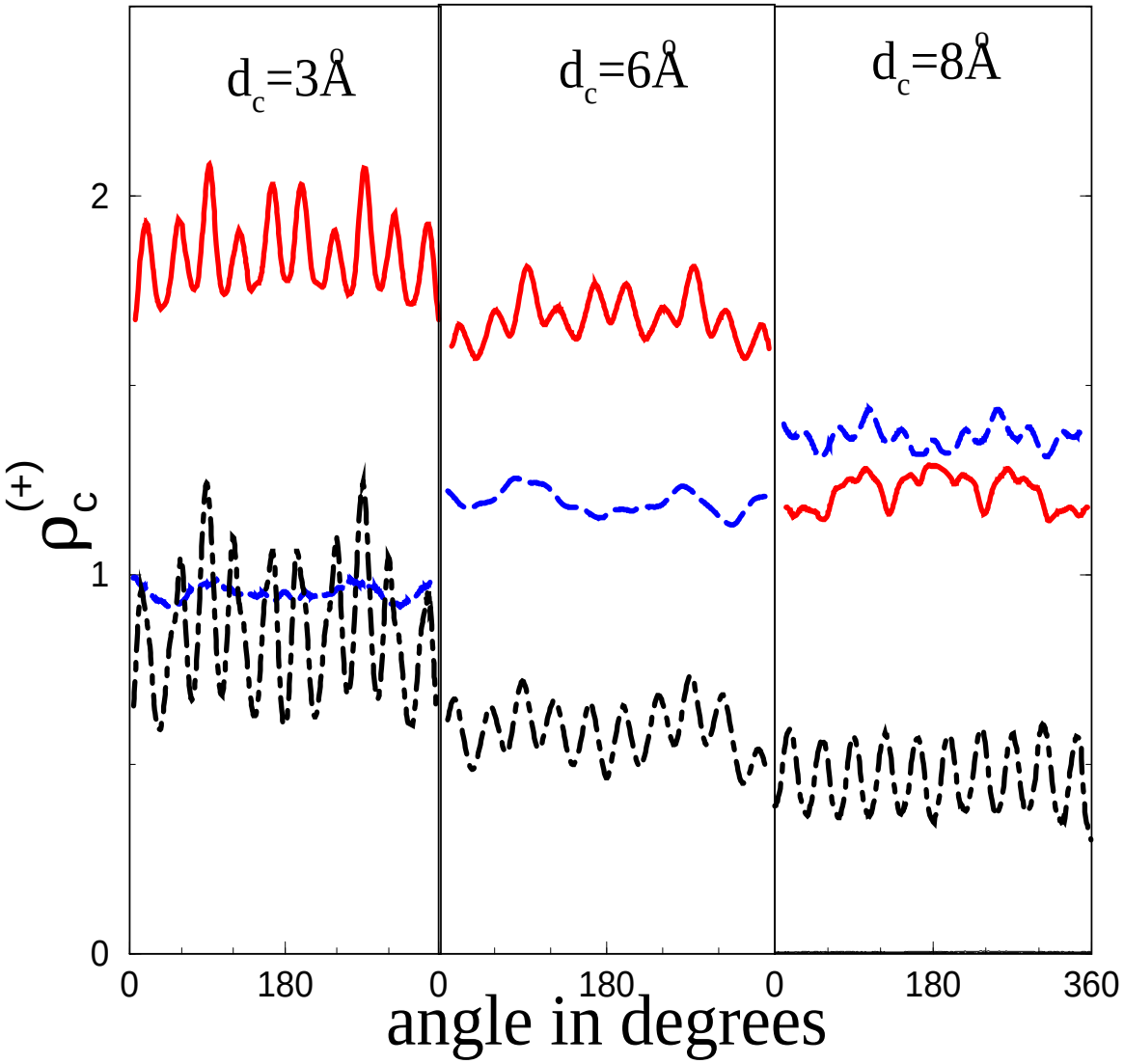

FIG. 14. Panoramic view of cation density near DNA surface for $q_c = 1$, $q_s = 1$ (Set 1), C_s =0.1 Mol/l and the MAM. Different cation diameters, from left to right: $d_c = 3$Å, $d_c = 6$Å, $d_c = 8$Å. Full line- cation distribution in the minor groove, dashed line- cation distribution in the major groove, dot-dashed line- cation distribution on the phosphate strands. Note that the the cation adsorption in the major groove exceeds the cation adsorption in the minor groove for $d_c = 8$Å, collate the full and dashed lines in the rigth side of figure.